Geophys. J. Int. (2006) doi: 10.1111/j.1365-246X.2006.03009.x

Scaling properties of convection-driven dynamos in rotating spherical shells and application to planetary magnetic fields

U. R. Christensen[1] and J. Aubert[2]

[1]*Max-Planck-Institut für Sonnensystemforschung, Katlenburg-Lindau, Germany. E-mail: christensen@mps.mpg.de*
[2]*Institut de Physique du Globe de Paris, Paris, France*

Accepted 2006 March 17. Received 2006 March 17; in original form 2005 September 28

SUMMARY

We study numerically an extensive set of dynamo models in rotating spherical shells, varying all relevant control parameters by at least two orders of magnitude. Convection is driven by a fixed temperature contrast between rigid boundaries. There are two distinct classes of solutions with strong and weak dipole contributions to the magnetic field, respectively. Non-dipolar dynamos are found when inertia plays a significant role in the force balance. In the dipolar regime the critical magnetic Reynolds number for self-sustained dynamos is of order 50, independent of the magnetic Prandtl number Pm. However, dynamos at low Pm exist only at sufficiently low Ekman number E. For dynamos in the dipolar regime we attempt to establish scaling laws that fit our numerical results. Assuming that diffusive effects do not play a primary role, we introduce non-dimensional parameters that are independent of any diffusivity. These are a modified Rayleigh number based on heat (or buoyancy) flux Ra_Q^*, the Rossby number Ro measuring the flow velocity, the Lorentz number Lo measuring magnetic field strength, and a modified Nusselt number Nu^* for the advected heat flow. To first approximation, all our dynamo results can be collapsed into simple power-law dependencies on the modified Rayleigh number, with approximate exponents of $2/5$, $1/2$ and $1/3$ for the Rossby number, modified Nusselt number and Lorentz number, respectively. Residual dependencies on the parameters related to diffusion (E, Pm, Prandtl number Pr) are weak. Our scaling laws are in agreement with the assumption that the magnetic field strength is controlled by the available power and not necessarily by a force balance. The Elsasser number Λ, which is the conventional measure for the ratio of Lorentz force to Coriolis force, is found to vary widely. We try to assess the relative importance of the various forces by studying sources and sinks of enstrophy (squared vorticity). In general Coriolis and buoyancy forces are of the same order, inertia and viscous forces make smaller and variable contributions, and the Lorentz force is highly variable. Ignoring a possible weak dependence on the Prandtl numbers or the Ekman number, a surprising prediction is that the magnetic field strength is independent both of conductivity and of rotation rate and is basically controlled by the buoyancy flux. Estimating the buoyancy flux in the Earth's core using our Rossby number scaling and a typical velocity inferred from geomagnetic secular variations, we predict a small growth rate and old age of the inner core and obtain a reasonable magnetic field strength of order 1 mT inside the core. From the observed heat flow in Jupiter, we predict an internal field of 8 mT, in agreement with Jupiter's external field being 10 times stronger than that of the Earth.

Key words: convection, core flow, dynamo theory, geomagnetic field, inner core, planetology.

1 INTRODUCTION

In the past 10 yr numerical models of convection-driven dynamos in rotating spherical shells have been successful in reproducing the main properties of the geomagnetic field, including the dipole dominance and approximate dipole strength, details of the field morphology at the outer boundary of the dynamo region, secular variation of the magnetic field and stochastic dipole reversals resembling those seen in the paleomagnetic record (Kageyama *et al.* 1995; Glatzmaier & Roberts 1995a,b; Kuang & Bloxham 1997; Christensen *et al.* 1998; Busse *et al.* 1998; Christensen *et al.* 1999; Kuang & Bloxham 1999; Takahashi *et al.* 2005). Dynamo models have been used to investigate the possible field generation mechanism in the Earth's core

(Olson *et al.* 1999; Ishihara & Kida 2002), the influence of lower mantle heterogeneity on magnetic field properties (Glatzmaier *et al.* 1999; Bloxham 2000a,b; Olson & Christensen 2002; Bloxham 2002; Christensen & Olson 2003; Kutzner & Christensen 2004) and the generation of planetary magnetic fields that differ in geometry (Uranus, Neptune) or strength (Mercury) from the Earth's field (Stanley & Bloxham 2004; Stanley *et al.* 2005).

However, for practical reasons the values of some of the control parameters in the dynamo models differ strongly from planetary values. In particular, the Ekman number that measures the relative importance of viscous forces to Coriolis forces is typically five to ten orders of magnitude too large, depending on whether molecular or 'turbulent' viscosities are assumed, and the magnetic Prandtl number, the ratio of viscosity to magnetic diffusivity, is six orders of magnitude larger than the appropriate value for liquid iron. Therefore, it remains doubtful if the flow regime in the numerical models is basically the same as in planetary cores or if the agreement with the Earth's magnetic field is rather fortuitous.

One way to assess the relevance of the dynamo models is to determine how their characteristic properties depend on the control parameters. Systematic parameter studies have been started by Christensen *et al.* (1999), Grote *et al.* (2000) and Simitev & Busse (2005). The main aim of these studies has been to determine in which parts of the parameter space dynamo solutions exist and what their fundamental magnetic field geometry is. The results show an influence of the mechanical boundary conditions and the mode of driving convection. For rigid boundaries and a strong source of buoyancy at the inner core boundary, the magnetic field outside the fluid shell is dominated by the axial dipole component at moderately supercritical values of the Rayleigh number, but is small scaled with a weak dipole component at strongly supercritical values (Kutzner & Christensen 2002). With stress-free boundaries and/or a strong component of driving by volumetric heat sources, dipole-dominated solutions give way to a non-dipolar magnetic fields (quadrupolar, small scaled or magnetic fields restricted to one hemisphere), in particular at lower values of the magnetic Prandtl number (Grote *et al.* 1999, 2000; Kutzner & Christensen 2000; Simitev & Busse 2005). Christensen *et al.* (1999) found that the minimum value of the magnetic Prandtl number at which dynamo solutions exist depends on the Ekman number. Dynamos at low, that is, more realistic, values of the magnetic Prandtl number are found only at low enough Ekman number, which makes their study computationally very demanding.

The next step toward understanding the dynamo process and to ascertain if the numerical models can be applied to planetary conditions is to derive scaling laws that relate characteristic properties of the dynamo solutions to the control parameters. Before, such scaling laws have been suggested on the basis of physical reasoning with little or no reference to actual dynamo solutions (e.g. Stevenson 1979; Starchenko & Jones 2002). Finding scaling laws for the magnetohydrodynamic dynamo problem is a particularly difficult task, because it is governed by at least four relevant control parameters and because the relative importance of the various forces on the flow (inertia, Coriolis force, Lorentz force, viscosity, buoyancy) may change over the accessible parameter range, which could prevent a unique scaling relation. For flow in planetary cores it is usually assumed that inertia and in particular viscosity play a negligible role and that the primary forces balance is between Coriolis force, Lorentz force, buoyancy and pressure gradient forces (magnetostrophic or MAC balance). A systematic numerical study of non-magnetic convection in a rotating shell with stress-free boundaries (Christensen 2002) has suggested that a regime in which viscous forces become unimportant can actually be approached with the present-day computational means and asymptotic scaling laws have been derived for the limit of small Ekman number. With the Lorentz force lacking, inertia retains an important role to balance the Coriolis forces in this case (Aubert *et al.* 2001). A first step in finding scaling laws from numerical dynamo solutions has been made by Christensen & Tilgner (2004), who derived a relation between the magnetic dissipation time, describing the rate at which magnetic energy is destroyed by Ohmic dissipation, and the magnetic Reynolds number, a measure for the flow velocity in terms of shell thickness and magnetic diffusion time. Based on the numerical results alone Christensen & Tilgner (2004) could not exclude a weak additional dependence on the magnetic Prandtl number, but by using results from the Karlsruhe laboratory dynamo experiment (Stieglitz & Müller 2001; Müller *et al.* 2004) they concluded that this dependency is absent or vanishes at small values of the magnetic Prandtl number. Aubert (2005) studied the zonal flow velocity in non-magnetic convection and in dynamos and found distinct scaling laws that indicate a different balance of forces in the two cases. In the dynamo case both viscosity and inertia were found to be unimportant, suggesting that at least the zonal flow is in a magnetostrophic balance.

In this paper we use an extensive set of numerical dynamo results in order to derive scalings for the mean flow velocity, the heat transport and the magnetic field strength. We restrict the analysis to dynamos that generate a dipole-dominated magnetic field.

2 GOVERNING EQUATIONS AND NON-DIMENSIONAL PARAMETERS

For numerical modelling the equations of convection-driven magnetohydrodynamic flow and electromagnetic induction in an electrically conducting, rotating spherical shell are usually cast into non-dimensional form. However, different schemes for non-dimensionalization are possible. Conventionally, time is scaled by some diffusion time, where the choice is between viscous, thermal or magnetic diffusivity. Based on the hypothesis that diffusive processes do not play a primary role, in contrast to the effects of rotation, we follow the path introduced by Christensen (2002) and Aubert (2005) and select the inverse rotation frequency Ω^{-1} of the shell as the basic timescale. Length scale is the shell thickness D, the non-hydrostatic pressure Π is scaled by $\rho\Omega^2 D^2$, where ρ is the density, and the scale for temperature is ΔT, the imposed temperature difference between the isothermal inner boundary at radius r_i and outer boundary at r_o. Here, we fix the ratio $\eta = r_i/r_o$ to 0.35. For dynamo problems in rotating systems the magnetic induction B is frequently scaled by $(\rho\mu\lambda\Omega)^{1/2}$ with μ the magnetic permeablity and λ the magnetic diffusivity. This choice makes the square of the mean non-dimensional magnetic field strength equal to the Elsasser number

$$\Lambda = B_{\rm rms}^2 \big/ \rho\mu\lambda\Omega, \tag{1}$$

which is considered to represent the ratio of Lorentz forces to Coriolis forces acting on the flow. Here we follow again a different path and select $(\rho\mu)^{1/2}\ \Omega D$ for scaling B. With this choice none of the diffusivites appears in any of the scales and the governing equations in the Boussinesq approximation can be written in a rather simple and symmetric form:

$$\frac{\partial \mathbf{u}}{\partial t} + \mathbf{u}\cdot\nabla\mathbf{u} + 2\hat{\mathbf{z}}\times\mathbf{u} + \nabla\Pi = E\nabla^2\mathbf{u} + Ra^*\frac{\mathbf{r}}{r_o}T + (\nabla\times\mathbf{B})\times\mathbf{B}, \tag{2}$$

$$\frac{\partial \mathbf{B}}{\partial t} - \nabla \times (\mathbf{u} \times \mathbf{B}) = E_\lambda \nabla^2 \mathbf{B}, \tag{3}$$

$$\frac{\partial T}{\partial t} + \mathbf{u} \cdot \nabla T = E_\kappa \nabla^2 T, \tag{4}$$

$$\nabla \cdot \mathbf{u} = 0, \quad \nabla \cdot \mathbf{B} = 0. \tag{5}$$

Here the unit vector $\hat{\mathbf{z}}$ indicates the direction of the rotation axis and gravity varies linearly with the radius $\mathbf{r}$. The four non-dimensional control parameters are the (viscous) Ekman number

$$E = \frac{\nu}{\Omega D^2}, \tag{6}$$

the magnetic Ekman number

$$E_\lambda = \frac{\lambda}{\Omega D^2} = \frac{E}{Pm}, \tag{7}$$

the thermal Ekman number

$$E_\kappa = \frac{\kappa}{\Omega D^2} = \frac{E}{Pr}, \tag{8}$$

and the modified Rayleigh number

$$Ra^* = \frac{\alpha g_o \Delta T}{\Omega^2 D}, \tag{9}$$

where ν is viscosity, κ thermal diffusivity, α thermal expansivity and g_o gravity at the outer radius r_o. In our scaling, the diffusive terms in eqs (2)–(4) multiply with the respective Ekman numbers, the buoyancy term is multiplied with a modified Rayleigh number that is independent of any diffusivity, and all other terms are parameter free. In place of the magnetic and thermal Ekman numbers we will later use the more conventional hydrodynamic Prandtl number $Pr = \nu/\kappa$ and magnetic Prandtl number $Pm = \nu/\lambda$.

We are interested in how characteristic values of the non-dimensional velocity and of the non-dimensional magnetic field strength depend on the control parameters. The kinetic energy and the magnetic energy, scaled by $\rho\Omega^2 D^5$, are given by

$$E_{\rm kin} = \frac{1}{2} \int \mathbf{u} \cdot \mathbf{u} \, dV, \tag{10}$$

and

$$E_{\rm mag} = \frac{1}{2} \int \mathbf{B} \cdot \mathbf{B} \, dV, \tag{11}$$

respectively, where the integral is taken over the fluid shell in case of eq. (10) and over all space in case of eq. (11). The characteristic mean velocity is the Rossby number,

$$Ro = \left(\frac{2E_{\rm kin}}{V_s} \right)^{1/2}, \tag{12}$$

and we call the characteristic non-dimensional magnetic field strength the Lorentz number

$$Lo = \left(\frac{2E_{\rm mag}}{V_s} \right)^{1/2}, \tag{13}$$

where V_s is the volume of the spherical shell. The relation between the Elsasser number and the Lorentz number is given by

$$\Lambda = Lo^2 Pm E^{-1}. \tag{14}$$

In a regime where diffusive processes do not play a major role, the Rossby number and the Lorentz number are expected to depend on the modified Rayleigh number rather than on the conventional Rayleigh number

$$Ra = \frac{Ra^*}{E_\kappa E}. \tag{15}$$

To obtain a non-dimensional measure for convective heat transport that is independent of the thermal diffusivity we use a modified Nusselt number

$$Nu^* = \frac{1}{4\pi r_o r_i} \frac{Q_{\rm adv}}{\rho c \Delta T \Omega D}, \tag{16}$$

where the advected heat flow $Q_{\rm adv}$ is the time-average total heat flow Q minus the conductive heat flow $Q_{\rm cond} = 4\pi r_o r_i \rho c \, \kappa \Delta T / D$ and c is the heat capacity. The relation to the conventional Nusselt number

$$Nu = \frac{1}{4\pi r_o r_i} \frac{Q D}{\rho c \kappa \Delta T}, \tag{17}$$

is given by

$$Nu^* = (Nu - 1) E_\kappa. \tag{18}$$

Note that the modified Nusselt number used here is based on the advective heat flux alone, in contrast to the definition employed by Christensen (2002) and Aubert (2005).

Finally, although the solutions have been calculated for a fixed temperature contrast, we analyse our results in terms of a modified Rayleigh number Ra^*_Q based on the advected heat flux rather than on ΔT

$$Ra^*_Q = \frac{1}{4\pi r_o r_i} \frac{\alpha g_o Q_{\rm adv}}{\rho c \Omega^3 D^2}. \tag{19}$$

The relation between the various Rayleigh numbers is $Ra^*_Q = Ra^* Nu^* = Ra(Nu - 1) E_\kappa^2 \, E$.

Considering more general sources of buoyancy, we can replace the heat flux by the buoyancy flux, or mass anomaly flux, Q_B, which in case of thermal buoyancy is given by $Q_B = \alpha Q_{\rm adv}/c$. The Rayleigh number

$$Ra^*_B = \frac{1}{4\pi r_o r_i} \frac{g_o Q_B}{\rho \Omega^3 D^2}, \tag{20}$$

is a non-dimensional expression for the buoyancy flux. In case of thermal convection it is identical to Ra^*_Q.

For planetary applications the flux-based Rayleigh numbers are more convenient, since estimates for the heat flux or buoyancy flux exist, whereas the (superadiabatic) temperature contrast is not known. Moreover, Ra^*_Q is very closely connected to the power P generated by buoyancy forces (scaled by $\rho\Omega^3 D^5$)

$$P = Ra^* \int \frac{r}{r_o} u_r T \, dV. \tag{21}$$

In the appendix we show that to a very good approximation

$$P = 2\pi\eta \frac{1+\eta}{(1-\eta)^2} Ra^*_Q \quad \approx \quad 7.01 Ra^*_Q. \tag{22}$$

The rate of Ohmic dissipation is given by

$$D_\lambda = E_\lambda \int (\nabla \times \mathbf{B})^2 \, \mathbf{dV}. \tag{23}$$

For our models we calculate the time-average fraction of Ohmic dissipation

$$f_{\rm ohm} = D_\lambda / P. \tag{24}$$

We employ rigid mechanical boundary conditions and assume no heat sources inside the fluid shell, which is more favourable to obtain dipole-dominated dynamo solutions. The magnetic field is matched to a potential field outside the fluid shell and in most cases also to a potential field inside the (insulating) inner core. In some cases we assumed a conducting inner core, with a ratio $r_\lambda = 1$ of outer core diffusivity to inner core diffusivity. This requires the solution

of eq. (3) for $\mathbf{u} = 0$ in this region. Wicht (2002) found only small differences between the two options and we confirmed this in a few cases that have been run with both kinds of conditions.

The equations are solved by a spectral transform method described in Glatzmaier (1984), Christensen *et al.* (1999) or Tilgner (1999). The resolution in terms of the maximum harmonic degree and order $\ell_{\max}$ and number of radial grid levels N_r was selected so that a drop by a factor of 50 or more is found in the kinetic and magnetic energy spectra from the maximum to the energy at the cut-off wavelength. This resolution has been found to be sufficient for the robust determination of characteristic mean properties of the solution (Christensen *et al.* 1999; Kutzner & Christensen 2002). At larger values of the Ekman number, solutions are calculated for a full sphere (symmetry parameter $m_s = 1$), at lower values two-fold symmetry in longitude ($m_s = 2$) and at the lowest Ekman numbers four-fold symmetry ($m_s = 4$) is used to save computer time. Comparing results for different symmetries in a few cases showed no significant influence on the average properties of the dynamos.

Usually a solution obtained at different parameters served as initial condition. The run time $t_{\rm run}$ of each case covers at least 50 advection times, where one advection time unit is the shell thickness divided by the rms velocity. An exception is a case at the lowest Ekman number that we reached, which was run for only 28 advection times, but seems to have equilibrated. The transient adjustment to the new condition occurs in about 5 to 20 advection time units after which a statistically equilibrated solution is established. We reject the first part of the time-series, typically about 20 advection times, and for the remainder we average in time several properties of interest to obtain characteristic values. In particular, we calculate time-average values of the Rossby number *Ro*, the Lorentz number *Lo*, the modified Nusselt number Nu^*, the power *P*, and the fraction of Ohmic dissipation $f_{\rm ohm}$. In addition, we determine the relative dipole field strength $f_{\rm dip}$, defined as the time-average ratio on the outer shell boundary of the mean dipole field strength to the field strength in harmonic degrees $\ell = 1$–12, and the ratio $b_{\rm dip}$ of the mean field strength inside the shell to the dipole strength on the outer boundary.

3 RESULTS

The data base for this study has been built over several years. Some of the results have been published in Christensen *et al.* (1999), Kutzner & Christensen (2000), Kutzner & Christensen (2002), Christensen & Tilgner (2004) and Aubert (2005), although previous cases have been rerun to obtain additional data that had not been recorded before or to get a more representative time average. Additional, not previously reported, cases have been calculated in particular to extend the data base to smaller Ekman numbers and magnetic Prandtl numbers and to hydrodynamic Prandtl numbers different from one. For a detailed analysis we selected from this data base cases that satisfy the following criteria:

(1) The dynamo generates a non-decaying and dipole-dominated magnetic field. The latter condition is met when the relative dipole strength $f_{\rm dip}$ exceeds 0.35.

(2) The Ekman number is 3×10^{-4} or smaller. The lowest value of the Ekman number is 10^{-6}. We note that our definition of the Ekman number is conservative; with the definition of Kono & Roberts (2002), $E' = \nu/(2\Omega r_o^2)$, the range is roughly from 2×10^{-7} to 6×10^{-5}.

(3) Convection must be sufficiently vigorous and fill the entire volume. For this we require $Nu > 2$, which normally implies that the Rayleigh number exceeds the critical value by a factor of five or more. We list critical values of the Rayleigh number $Ra_{\rm crit}$ and the critical azimuthal wavenumber $m_{\rm crit}$ in Table 1.

Table 1. Critical Rayleigh number.

E	Pr	$Ra_{\rm crit}$	$Ra^*_{\rm crit}$	$m_{\rm crit}$
3×10^{-4}	3.0	2.391×10^5	7.173×10^{-3}	5
3×10^{-4}	1.0	2.026×10^5	1.823×10^{-2}	5
3×10^{-4}	0.3	1.373×10^5	4.119×10^{-2}	5
10^{-4}	10	9.410×10^5	9.410×10^{-4}	7
10^{-4}	3	8.627×10^5	2.876×10^{-3}	8
10^{-4}	1.0	6.965×10^5	6.965×10^{-3}	8
10^{-4}	0.3	4.407×10^5	1.469×10^{-2}	7
10^{-4}	0.1	2.865×10^5	2.865×10^{-2}	6
3×10^{-5}	3.0	3.674×10^6	1.102×10^{-3}	12
3×10^{-5}	1.0	2.833×10^6	2.550×10^{-3}	11
3×10^{-5}	0.3	1.684×10^6	5.052×10^{-3}	10
3×10^{-5}	0.1	1.047×10^6	9.423×10^{-3}	8
10^{-5}	3.0	1.426×10^7	4.753×10^{-4}	16
10^{-5}	1.0	1.057×10^7	1.057×10^{-3}	15
3×10^{-6}	3.0	6.475×10^7	1.943×10^{-4}	22
3×10^{-6}	1.0	4.591×10^7	4.132×10^{-4}	22
10^{-6}	1.0	1.791×10^8	1.791×10^{-4}	31

We have 66 different dynamos that satisfy the three criteria, covering at least two orders of magnitude in all control parameters. The modified Rayleigh number Ra^* is in the range of 0.001–0.4, or between 5 and 50 times supercritical. The magnetic Prandtl number ranges between 0.06 and 10 and the hydrodynamic Prandtl number falls between 0.1 and 10. In terms of mean-field dynamo theory, our dipolar solutions can be classified as α^2-dynamos (Olson *et al.* 1999). Differential rotation is weak, the toroidal magnetic field is of similar strength as the poloidal field and the axisymmetric toroidal field is usually weaker than the axisymmetric poloidal field, except inside the inner core tangent cylinder. The results for the selected cases are summarized in Table 2.

3.1 Dynamo regimes

Before we turn to the scaling laws for dipole-dominated dynamos, we first revisit the question of the existence of dynamo solutions and the class of magnetic field that they produce, following up earlier studies with a more extensive data basis. In Fig. 1 we show for a fixed Prandtl number of one and various values of the Ekman number the type of solution obtained in dependence of the Rayleigh number and the magnetic Prandtl number. Here we note that close to the regime boundaries the transient adjustment of the magnetic field may take longer than 50 advective time units and is more typically on the magnetic diffusion timescale. When in doubt we, therefore, run a case twice, starting from different initial magnetic field structures.

First we confirm the earlier result (Christensen *et al.* 1999) that the minimum magnetic Prandtl number at which dynamos exist, at least those generating a dipole-dominated magnetic field, increases with the Ekman number. In Fig. 2(a) we plot for $Pr = 1$ the lowest magnetic Prandtl number at which we found a dipolar dynamo as a function of Ekman number. The solid line for the minimum magnetic Prandtl number is given by the relation suggested in Christensen *et al.* (1999) on the basis of results restricted to Ekman numbers $E \geq 10^{-4}$:

$$Pm_{\min} = 450 E^{0.75}. \tag{25}$$

Table 2. Results.

Ra^*	Pr	Pm	r_λ	$\ell_{\max}$	N_r	m_s	$t_{\rm run}$	Ro	$\bar{\ell}_u$	Nu	Lo	$f_{\rm dip}$	$b_{\rm dip}$	$f_{\rm ohm}$
							$E = 1 \times 10^{-6}$							
0.0011	1.0	1.000	0	201	81	4	162 000	1.72×10^{-4}	42	2.18	7.78×10^{-4}	0.87	4.9	0.80
							$E = 3 \times 10^{-6}$							
0.0198	1.0	0.060	0	224	97	4	13 000	3.98×10^{-3}	55	17.80	4.02×10^{-3}	0.98	3.0	0.41
0.0162	1.0	0.075	0	224	97	4	15 000	3.34×10^{-3}	56	14.90	3.51×10^{-3}	0.96	3.2	0.40
0.0072	1.0	0.100	0	201	81	4	42 000	1.53×10^{-3}	56	5.33	1.50×10^{-3}	0.99	3.0	0.25
0.0090	1.0	0.100	0	201	81	4	28 000	1.90×10^{-3}	59	7.57	2.16×10^{-3}	0.95	3.2	0.34
0.0162	1.0	0.100	0	224	97	4	29 000	3.27×10^{-3}	58	14.90	3.61×10^{-3}	0.92	3.4	0.44
0.0045	1.0	0.500	0	168	81	4	85 000	7.71×10^{-4}	46	3.50	1.96×10^{-3}	0.82	5.3	0.62
0.0090	1.0	0.500	0	201	81	4	34 000	1.48×10^{-3}	49	7.33	3.61×10^{-3}	0.87	5.1	0.67
0.0162	1.0	0.500	0	224	97	4	22 000	2.36×10^{-3}	45	12.70	5.72×10^{-3}	0.92	4.9	0.74
0.0021	3.0	1.000	0	168	81	4	119 000	4.18×10^{-4}	56	5.09	1.12×10^{-3}	0.68	6.5	0.47
0.0036	1.0	1.000	0	168	81	4	92 000	5.52×10^{-4}	35	2.95	2.11×10^{-3}	0.89	5.5	0.76
0.0015	3.0	1.500	0	168	81	4	188 000	2.68×10^{-4}	47	3.57	1.08×10^{-3}	0.81	5.3	0.60
							$E = 1 \times 10^{-5}$							
0.0500	1.0	0.100	0	168	81	2	6100	8.49×10^{-3}	36	14.40	7.83×10^{-3}	0.96	2.8	0.39
0.0350	1.0	0.150	0	168	81	2	12 000	5.93×10^{-3}	39	11.30	7.73×10^{-3}	0.96	3.0	0.45
0.0110	1.0	0.200	0	134	65	2	26 000	1.97×10^{-3}	37	2.92	1.91×10^{-3}	0.98	3.1	0.21
0.0150	1.0	0.200	0	134	65	2	20 000	2.54×10^{-3}	40	4.06	3.41×10^{-3}	0.95	3.3	0.33
0.0350	1.0	0.250	0	168	81	2	12 000	5.37×10^{-3}	38	10.80	8.86×10^{-3}	0.95	3.1	0.56
0.0500	1.0	0.250	0	168	81	2	12 000	6.93×10^{-3}	38	13.50	1.03×10^{-2}	0.96	3.2	0.58
0.0150	1.0	0.500	0	133	65	2	35 000	2.35×10^{-3}	36	4.61	5.03×10^{-3}	0.89	4.3	0.57
0.0350	1.0	0.500	0	168	81	2	18 000	4.56×10^{-3}	36	9.58	9.35×10^{-3}	0.94	3.7	0.66
0.0080	1.0	1.000	0	133	65	2	91 000	1.19×10^{-3}	25	2.47	3.31×10^{-3}	0.86	5.5	0.65
0.0117	3.0	1.500	0	168	81	2	34 000	1.48×10^{-3}	35	9.12	5.44×10^{-3}	0.94	4.1	0.67
0.0075	1.0	2.000	1	128	65	4	120 000	1.05×10^{-3}	23	2.65	4.14×10^{-3}	0.88	6.1	0.75
0.0100	1.0	2.000	1	128	65	4	120 000	1.22×10^{-3}	23	3.55	6.20×10^{-3}	0.89	4.8	0.81
0.0150	1.0	2.000	1	170	65	4	40 000	1.79×10^{-3}	26	5.41	8.95×10^{-3}	0.89	4.6	0.80
0.0200	1.0	2.000	1	170	81	4	45 000	2.34×10^{-3}	28	6.65	1.03×10^{-2}	0.87	5.1	0.79
0.0400	1.0	2.000	1	212	81	4	10 000	4.44×10^{-3}	32	10.70	1.21×10^{-2}	0.83	6.0	0.70
							$E = 3 \times 10^{-5}$							
0.0630	1.0	0.200	0	106	49	1	5200	1.01×10^{-2}	27	7.48	9.38×10^{-3}	0.96	2.8	0.31
0.0450	1.0	0.250	0	106	49	1	13 000	7.09×10^{-3}	28	5.63	9.07×10^{-3}	0.97	2.9	0.36
0.0720	1.0	0.250	0	133	65	1	13 000	1.09×10^{-2}	26	8.30	1.13×10^{-2}	0.94	2.9	0.38
0.0720	1.0	0.500	0	106	49	1	7000	8.95×10^{-3}	26	7.32	1.38×10^{-2}	0.95	3.5	0.54
0.0225	1.0	1.000	0	106	49	1	44 000	2.91×10^{-3}	20	2.75	7.51×10^{-3}	0.90	4.4	0.61
0.0750	0.3	1.000	0	106	49	2	13 000	8.36×10^{-3}	17	3.18	2.24×10^{-2}	0.85	4.7	0.76
0.1800	0.1	1.000	0	106	49	2	5000	2.13×10^{-2}	18	3.01	3.67×10^{-2}	0.73	6.6	0.69
0.0720	1.0	1.000	0	106	49	1	15 000	8.09×10^{-3}	24	7.18	1.56×10^{-2}	0.90	4.2	0.62
0.1080	1.0	1.000	0	133	65	1	17 000	1.17×10^{-2}	25	9.67	1.69×10^{-2}	0.87	4.7	0.57
0.0270	1.0	2.500	0	85	41	1	47 000	3.03×10^{-3}	17	3.64	1.34×10^{-2}	0.83	4.7	0.76
0.0720	1.0	2.500	0	106	49	1	20 000	7.53×10^{-3}	24	7.32	1.81×10^{-2}	0.78	5.6	0.63
0.1080	1.0	2.500	0	133	65	1	8300	1.11×10^{-2}	26	9.85	1.91×10^{-2}	0.74	6.6	0.56
0.0054	3.0	3.000	0	85	41	1	69 000	8.61×10^{-4}	20	2.13	2.03×10^{-3}	0.81	5.8	0.37
							$E = 1 \times 10^{-4}$							
0.0750	1.0	0.500	0	64	41	1	14 000	1.00×10^{-2}	18	3.25	1.22×10^{-2}	0.97	2.9	0.32
0.0750	1.0	1.000	0	64	41	1	9700	8.43×10^{-3}	16	3.06	1.68×10^{-2}	0.95	3.4	0.52
0.1500	1.0	1.000	0	85	41	1	6800	1.71×10^{-2}	18	5.28	1.95×10^{-2}	0.87	4.0	0.42
0.0750	1.0	2.000	0	106	49	1	23 000	8.27×10^{-3}	15	3.26	1.89×10^{-2}	0.86	4.3	0.59
0.1500	1.0	2.000	0	85	41	1	7700	1.65×10^{-2}	18	5.40	2.13×10^{-2}	0.75	5.3	0.45
0.3200	0.1	1.500	0	64	41	1	6700	3.61×10^{-2}	12	2.14	5.30×10^{-2}	0.66	7.1	0.58
0.1033	3.0	3.000	0	106	49	1	5300	0.98×10^{-2}	19	8.26	1.56×10^{-2}	0.80	4.8	0.42
0.1500	1.0	3.000	0	106	49	1	4800	1.57×10^{-2}	18	5.46	2.41×10^{-2}	0.70	6.1	0.49
0.0750	1.0	3.330	0	85	41	1	8100	8.29×10^{-3}	15	3.47	2.11×10^{-2}	0.74	5.2	0.59
0.0150	10.0	3.330	0	85	41	1	30 000	1.89×10^{-3}	20	5.22	5.13×10^{-3}	0.96	3.2	0.28
0.1500	1.0	5.000	0	106	49	1	3300	1.51×10^{-2}	17	5.43	2.64×10^{-2}	0.63	7.6	0.48
0.0667	3.0	6.000	0	106	49	1	12 000	6.56×10^{-3}	18	6.42	1.61×10^{-2}	0.74	5.5	0.50
0.0833	3.0	6.000	0	106	49	1	8500	7.95×10^{-3}	18	7.41	1.67×10^{-2}	0.70	6.1	0.46
0.1500	1.0	10.000	0	133	65	1	3500	1.45×10^{-2}	18	5.44	2.91×10^{-2}	0.55	10.1	0.46
0.0075	10.0	10.000	0	64	41	1	171 000	8.53×10^{-4}	15	3.10	5.38×10^{-3}	0.93	3.7	0.54
0.0150	10.0	10.000	0	85	41	1	37 000	1.57×10^{-3}	17	5.11	7.61×10^{-3}	0.88	4.1	0.49
0.0310	10.0	10.000	0	106	49	1	54 000	2.82×10^{-3}	18	8.10	9.54×10^{-3}	0.82	4.9	0.46

Table 2. (*Continued.*)

Ra^*	Pr	Pm	r_λ	$\ell_{\max}$	N_r	m_s	$t_{\rm run}$	Ro	$\bar{\ell}_u$	Nu	Lo	$f_{\rm dip}$	$b_{\rm dip}$	$f_{\rm ohm}$
							$E = 3 \times 10^{-4}$							
0.1125	1.0	1.500	0	42	33	1	10 000	1.23×10^{-2}	11	2.18	2.09×10^{-2}	0.92	3.5	0.42
0.1125	1.0	3.000	0	42	33	1	5500	1.15×10^{-2}	10	2.20	2.48×10^{-2}	0.80	4.5	0.50
0.3750	0.3	3.000	0	64	41	1	2400	4.11×10^{-2}	10	2.35	4.58×10^{-2}	0.53	8.6	0.43
0.1890	1.0	3.000	0	64	41	1	115 000	1.99×10^{-2}	12	3.11	2.71×10^{-2}	0.67	5.3	0.39
0.2250	1.0	3.000	0	64	41	1	13 000	2.45×10^{-2}	13	3.51	2.40×10^{-2}	0.63	6.1	0.30
0.2430	1.0	3.000	0	64	41	1	27 000	2.77×10^{-2}	13	3.72	1.98×10^{-2}	0.59	7.3	0.22
0.0990	3.0	3.000	0	64	41	1	13 000	9.70×10^{-3}	13	3.92	1.79×10^{-2}	0.86	3.8	0.35
0.0990	3.0	9.000	0	64	41	1	11 000	9.65×10^{-3}	13	4.14	2.03×10^{-2}	0.62	6.2	0.38
0.2430	1.0	5.000	0	64	41	1	4500	2.38×10^{-2}	12	3.64	3.28×10^{-2}	0.57	7.6	0.38

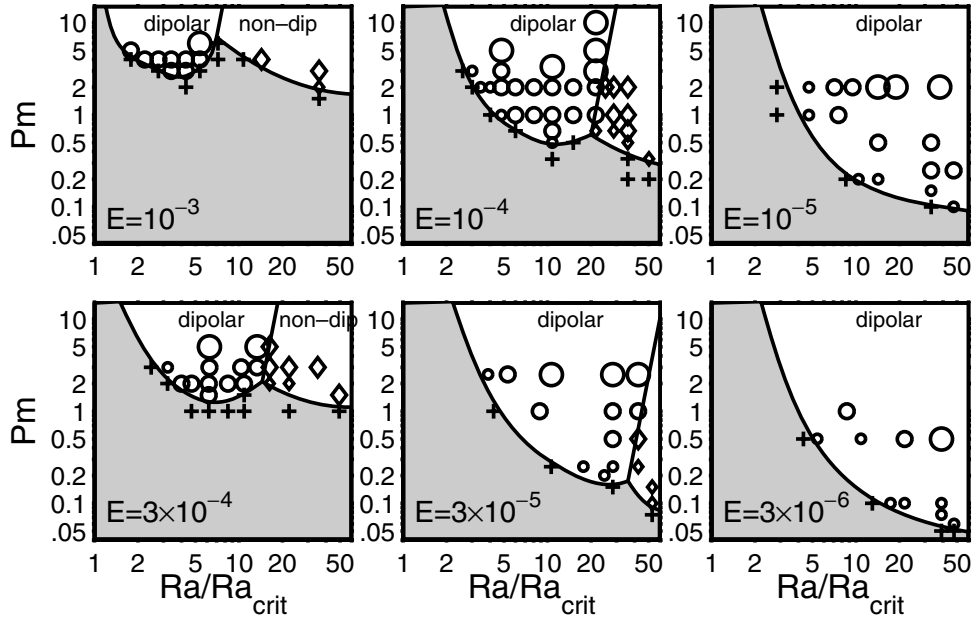

Figure 1. Regime diagram for dynamos at $Pr = 1$ with rigid boundaries driven by an imposed temperature contrast at different values of the Ekman number. Circles show dipolar dynamos, diamonds non-dipolar dynamos and crosses failed dynamos. The size of the symbol has been chosen according to the value of the Elsasser number. In parameter ranges not well covered by case studies the regime boundaries are tentative.

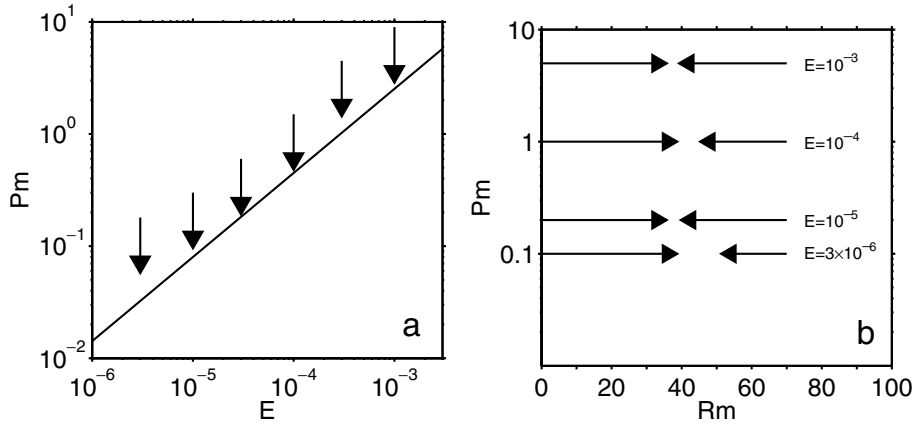

Figure 2. (a) The tip of the arrow indicates the lowest magnetic Prandtl number at which a non-decaying dipolar dynamo was found. Solid line according to eq. (25). (b) Tip of right arrow indicates lowest magnetic Reynolds number for self-sustained dipolar dynamos, left arrow highest magnetic Reynolds number for cases with decaying field. Intermediate cases have not been tested.

This relation is confirmed by the new results at lower Ekman number. At $E = 3 \times 10^{-6}$ the lowest magnetic Prandtl number at which we found a dynamo, $Pm = 0.06$, lies somewhat above the fitting line. However, from the systematic shift of the minimum Pm for dipolar dynamos towards higher supercritical Rayleigh number (Fig. 1), it seems likely that we have not reached the minimum, which may require a Rayleigh number more than 60 times supercritical at $E = 3 \times 10^{-6}$.

Since the hydrodynamic Prandtl number is one for all the cases considered here, eq. (25) holds also when the magnetic Prandtl number is replaced by the Roberts number $q = \kappa/\lambda = Pm/Pr$. Simitev & Busse (2005) noted that q may be a more relevant parameter than the magnetic Prandtl number. They found dynamos with a low Pm only in cases when Pr is also low and speculated that for $Pr \leq O(1)$ dynamo action occurs only at values of the Roberts number of order unity or larger, which is contradicted by our results.

Another question is whether the minimum value for self-sustained dynamo action of the magnetic Reynolds number

$$Rm = \frac{Ro}{E_\lambda} = \frac{u_{\rm rms}}{\lambda D}, \tag{26}$$

depends on Pm. For dynamos in non-rotating systems that generate a magnetic field from small-scale turbulence it had been found that the critical Reynolds number increases strongly when Pm is lowered below one and it has been debated if such dynamos exist at all for $Pm < 0.1$ (Schekochihin *et al.* 2004,2005). When a large-scale flow component is also present, low-Pm dynamos have been found (Ponty *et al.* 2005), but require a magnetic Reynolds number of the order 200, substantially higher than for dynamos at $Pm \approx 1$. In Fig. 2(b) we bracket the critical magnetic Reynolds number as function of the magnetic Prandtl number at appropriate values of the Ekman number. For the class of dynamos studied here, there is no strong dependence of the critical magnetic Reynolds number on Pm, provided the Ekman number is low enough. Our results are compatible with a nearly constant critical Rm of about 40–45.

Kutzner & Christensen (2002) found that the dipolar dynamo regime gives way to a class of dynamos that generate small-scale magnetic fields when the Rayleigh number is sufficiently increased with all other parameters held constant. The two regimes are clearly distinguished in the magnetic spectra at the outer boundary: the power is usually rather evenly distributed among the low-order harmonics, except for the dipole term, which is clearly stronger or clearly weaker, respectively, than the rest. When convection is driven by an imposed temperature contrast between the shell boundaries, as in the cases considered here, the transition is sharp, whereas for other modes of driving convection it can be more gradual. The degree of supercriticality of the Rayleigh number at which the transition occurs was found to increase when the Ekman number was lowered from 10^{-3} to 10^{-4} (Kutzner & Christensen 2002), thus making the parameter space domain of dipolar dynamos comparatively larger at low Ekman numbers. Here this trend is confirmed to continue for $E < 10^{-4}$ (Fig. 1). For the non-dipolar dynamos the critical magnetic Reynolds number is larger than 100. The dynamo mechanism in the non-dipolar regime seems, therefore, less efficient than in the dipolar regime.

Combining all results for different values of the Ekman number and the Prandtl numbers, we find non-dipolar dynamos at high values of the Rossby number and dipolar ones at low values, with some overlap of the two classes in the range $Ro \approx 1.5$–4×10^{-2}. The Rossby number can be considered as measuring the importance of inertial forces relative to the Coriolis force. Therefore, we hypothesize that the dipolar dynamo regime breaks down when inertia starts to play an essential role in the force balance. Sreenivasan & Jones (2006) observed a similar change of dynamo regime when they varied the two Prandtl numbers together at fixed values of the Ekman number and the Rayleigh number and attributed the change to the non-dipolar regime to the growing influence of inertial forces. They estimated that inertial effects become small when $Ro < 0.1$.

Because the inertial term in eq. (2) involves a length scale whereas the Coriolis term does not, a modified Rossby number that depends on the characteristic length scale of the flow rather than on the shell thickness is potentially a better measure for the balance between inertia and Coriolis force. Assuming that the radial and horizontal length scales are roughly similar, we estimate a characteristic value from the spectra of kinetic energy as function of spherical harmonic degree ℓ. The mean value $\bar{\ell}_u$ is obtained from the time-averaged kinetic energy spectrum

$$\bar{\ell}_u = \frac{\sum \ell \langle \mathbf{u}_\ell \cdot \mathbf{u}_\ell \rangle}{2E_{\rm kin}}, \tag{27}$$

where u_ℓ is the flow component at degree ℓ. As the mean radius to a point inside the shell is of order one, we set the characteristic half-wavelength of the flow to $\pi/\bar{\ell}_u$ and the modified Rossby number is

$$Ro_\ell = Ro\frac{\bar{\ell}_u}{\pi}. \tag{28}$$

In Fig. 3 we plot the relative dipole strength $f_{\rm dip}$ versus the modified Rossby number. We have included all cases, independent of the dipole strength, that satisfy the conditions (2) and (3) mentioned at the beginning of the section. There is a rather clear transition from the dipolar regime ($f_{\rm dip} > 0.5$) to the non-dipolar one ($f_{\rm dip} < 0.3$) at $Ro_\ell \approx 0.12$, irrespective of the values of the Ekman number, Prandtl number and magnetic Prandtl number. The only outlier is a non-dipolar case at $Ro_\ell \approx 0.09$. However, in this case the type of dynamo solution was sensitive to the starting condition. Depending on the initial magnetic field either a dipolar or a non-dipolar state persisted, the latter for 1.2 magnetic diffusion times (the two solutions are joined by a broken line in Fig. 3). In another case it took

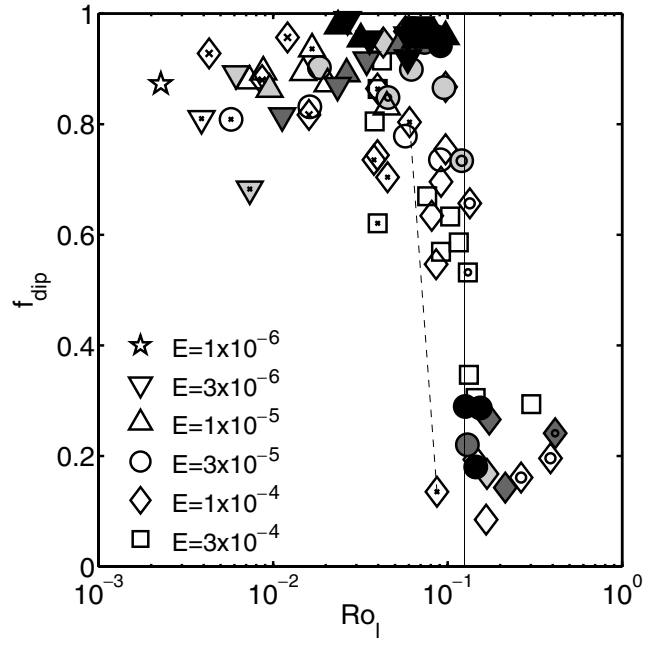

Figure 3. Relative dipole strength versus modified Rossby number. The Ekman number is indicated by the shape of the symbol and the magnetic Prandtl number by the shading ($Pm < 0.3$ black, $0.3 < Pm < 1$ dark grey, $Pm = 1$ light grey, $Pm > 1$ white). Hydrodynamical Prandtl numbers other than one are indicated by an additional small cross ($Pr = 3$), larger cross ($Pr = 10$), small circle ($Pr = 0.3$) or larger circle ($Pr = 0.1$) inside the main symbol. The two symbols joined by a broken line indicate a case where the dynamo regime depends on the starting condition.

approximately three magnetic diffusion times for the transition from a non-dipolar to a dipolar state to occur. Therefore, it is not clear if both branches of the solution are stable in the long term. In general the clear dependence of the regime on the modified Rossby number supports the assumption that inertial forces play the key role in the breakdown of dipolar dynamo solutions.

3.2 Heat transport

In Fig. 4(a) we plot in the conventional way the Nusselt number versus the Rayleigh number normalized by its critical value for all cases satisfying criteria (1)–(3). Of course the Nusselt number and Rayleigh number correlate, however, there is substantial scatter and the results do not fall on a single line. This changes remarkably when we plot the modified Nusselt number versus the flux-based modified Rayleigh number (Fig. 4b). We note that since both Nu^* and Ra_Q^* are defined in terms of the advected heat flux $Q_{\rm adv}$, the driving temperature contrast ΔT in eq. (16) assumes the role of the physical property that is determined by the functional dependence $Nu^*(Ra_Q^*)$. By the introduction of the modified 'diffusionless' parameters it is possible to collapse the data for all dynamos, regardless of the values of E, Pm and Pr, on a single regression line with a mean relative misfit of 5 per cent. We obtain the following power-law dependence

$$Nu^* = 0.076 Ra_Q^{*0.53}. \tag{29}$$

This is not much different from the scaling law obtained for non-magnetic rotating convection between stress-free boundaries, for which an exponent of 5/9 has been suggested (Christensen 2002). The exponent for the dependence of Nu^* on the Rayleigh number Ra^* based on ΔT is approximately 1.1. This very strong dependence compared to an exponent of order 1/3 that is typical for Benard-type convection seems to be a particular property of rotating convection. A requirement is that convection fills the entire fluid volume, that is, the Rayleigh number must be sufficiently supercritical (Tilgner & Busse 1997).

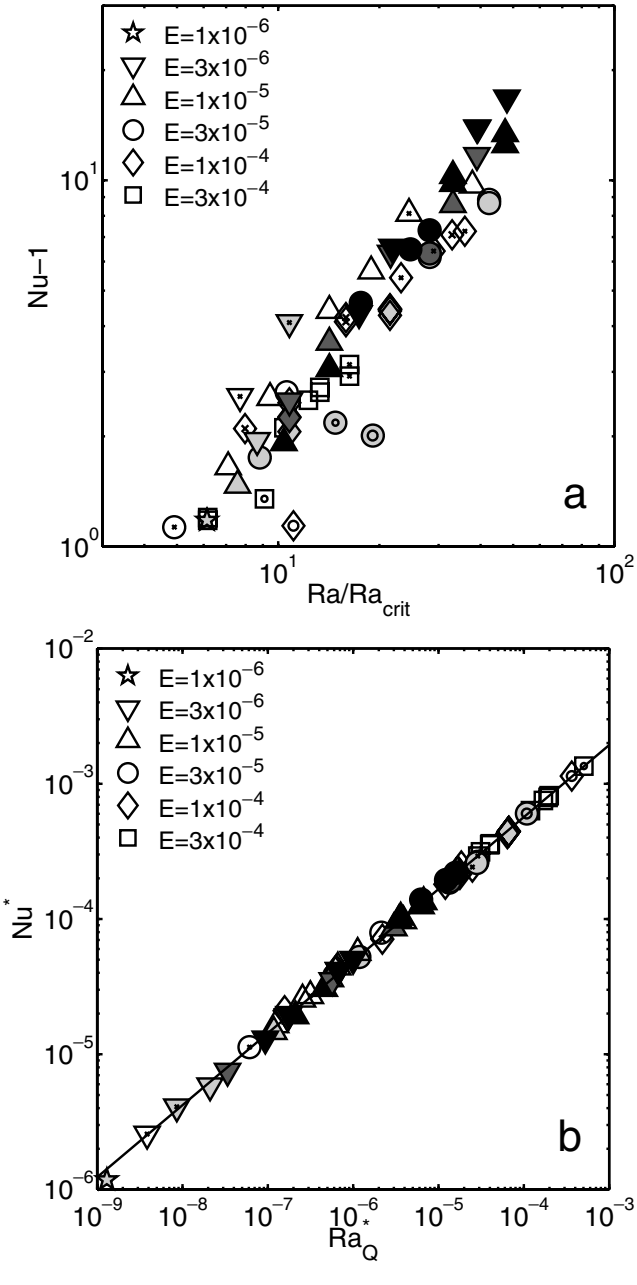

Figure 4. (a) Conventional Nusselt number versus Rayleigh number normalized by its critical value. (b) Modified Nusselt number versus modified flux-based Rayleigh number. Symbols as in Fig. 3.

3.3 Flow velocity

In Fig. 5 we plot the Rossby number, that is, the non-dimensional rms velocity, against the modified Rayleigh number. The best-fitting power law has the form

$$Ro = 0.85 Ra_Q^{*0.41}. \tag{30}$$

With a mean relative deviation of 18 per cent the fit is decent given that the cases cover a broad range of the control parameters E, Pm and Pr, and almost six decades in Ra_Q^*, but is not as good as in case of the Nusselt number.

We attempted to reduce the residual scatter by assuming an additional dependence on one more parameter. The best result is obtained

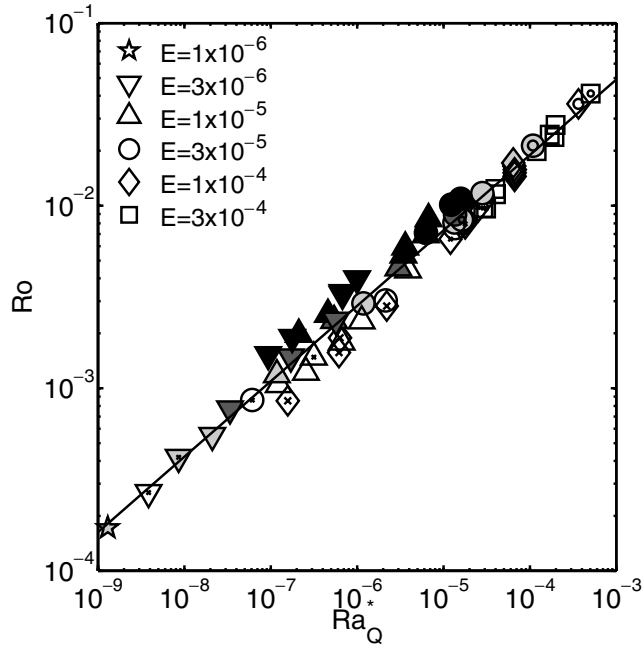

Figure 5. Rossby number versus modified Rayleigh number. Symbols as in Fig. 3.

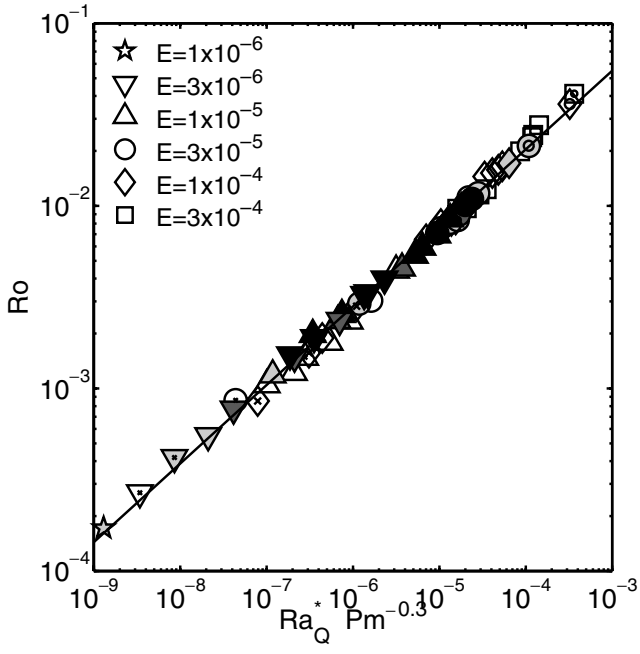

Figure 6. Rossby number versus a combination of modified Rayleigh number and magnetic Prandtl number. Symbols as in Fig. 3.

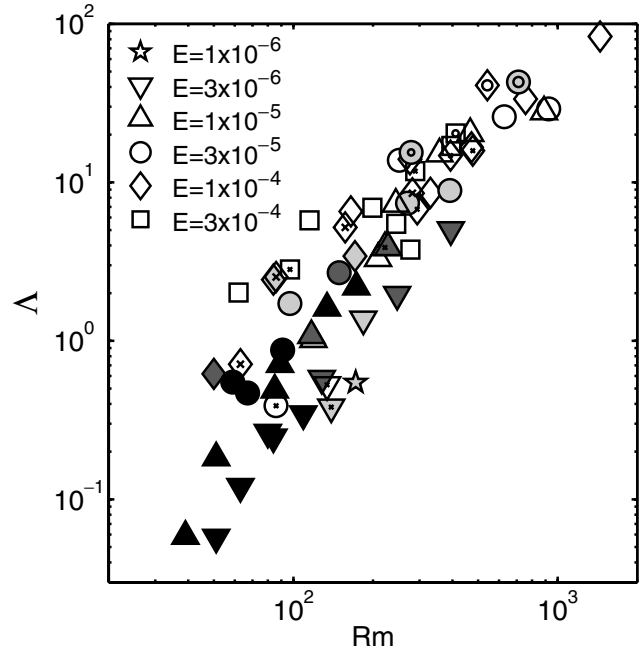

Figure 7. Elsasser number versus magnetic Reynolds number. Symbols as in Fig. 3.

with a two-parameter fit that involves the magnetic Prandtl number (Fig. 6), for which the optimal exponent is −0.13.

$$Ro = 1.07 Ra_Q^{*0.43} Pm^{-0.13}. \tag{31}$$

This reduces the mean deviation of the dynamo results from the fitting law to 8 per cent. The improvement is substantial, but not so large that a dependence on *Pm* can be firmly assumed. A similar improvement on including a dependence on *Pm* had been found by Christensen & Tilgner (2004) when scaling the magnetic diffusion time as function of the magnetic Reynolds number. However, based on results of a laboratory dynamo with a much lower *Pm* they rejected the additional dependence on the magnetic Prandtl number at least for $Pm \ll 1$.

3.4 Magnetic field strength

It is often assumed that in a magnetostrophic force balance the Elsasser number Λ should be of order one. For our dipole-dominated dynamos we find a broad range of values for the Elsasser number, between 0.06 and 100. There is some correlation with the magnetic Reynolds number *Rm* (Fig. 7), but clearly Λ does not simply depend on *Rm* alone. For a fixed value of *Rm*, the Elsasser number tends to decrease with decreasing Ekman number. The large range of values for Λ suggests that the dynamos are either not in a magnetostrophic balance or that the conventional Elsasser number is not a good measure for the degree of magnetostrophy.

A somewhat better fit is obtained when we relate the Lorentz number, that is, the non-dimensional mean magnetic field strength in our scaling, to the modified Rayleigh number (not shown). We do not discuss this results in detail, because a consideration based on the energetics of the dynamo suggests a correction term that significantly improves the fit to the numerical data. The fundamental idea is that the magnetic field strength is not determined by a force balance, but by the power available to balance Ohmic dissipation. Dissipation and magnetic field strength are linked through the length scale of the field, or a dissipation timescale, which we take as being a function of the flow properties. Christensen & Tilgner (2004) found an inverse relation between the magnetic dissipation time τ', that is, the ratio of magnetic energy $E_{\rm mag}$ to Ohmic dissipation D_λ, and the magnetic Reynolds number *Rm*. τ' is scaled with the magnetic diffusion time and by τ we denote the dissipation timescaled with the rotational timescale used here. From the relations $\tau = E_\lambda^{-1}\tau'$ and $Ro = E_\lambda Rm$ we find that $\tau \sim Ro^{-1}$. Furthermore, from eqs (13), (22) and (24) we obtain with $D_\lambda = f_{\rm ohm} P \sim f_{\rm ohm} Ra_Q^*$ and $Lo^2 = 2E_{\rm mag} = 2D_\lambda \tau$ the relation

$$\frac{Lo}{f_{\rm ohm}^{1/2}} \sim \left(\frac{Ra_Q^*}{Ro}\right)^{1/2}. \tag{32}$$

Using eq. (30) for the relation between Rossby number and Rayleigh number, a dependence of the Lorentz number, corrected for the fraction of Ohmic dissipation, on the modified Rayleigh number with an exponent of order 0.3 is predicted.

In Fig. 8 we plot the corrected Lorentz number against the modified Rayleigh number. For our selected dynamos the best-fitting power law is

$$\frac{Lo}{f_{\rm ohm}^{1/2}} = 0.92 Ra_Q^{*0.34}, \tag{33}$$

with a mean relative misfit of 17 per cent.

Again, as in the case of the Rossby number, the fit can be improved by assuming a weak additional dependence on the magnetic Prandtl number. A two-parameter best fit (Fig. 9) results in

$$\frac{Lo}{f_{\rm ohm}^{1/2}} = 0.76 Ra_Q^{*0.32} Pm^{0.11}. \tag{34}$$

The reduction of the misfit, to 10 per cent, is not as strong as in the case of the Rossby number.

3.5 Robustness of the scaling laws

We have found that the Rossby number and the Lorentz depend on the modified Rayleigh number through a power law. They may

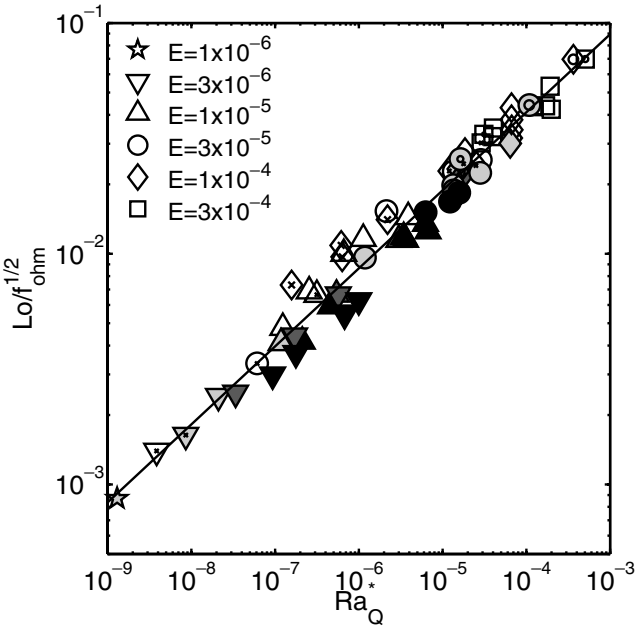

Figure 8. Lorentz number corrected for the relative fraction of Ohmic dissipation versus modified Rayleigh number. Symbols as in Fig. 3.

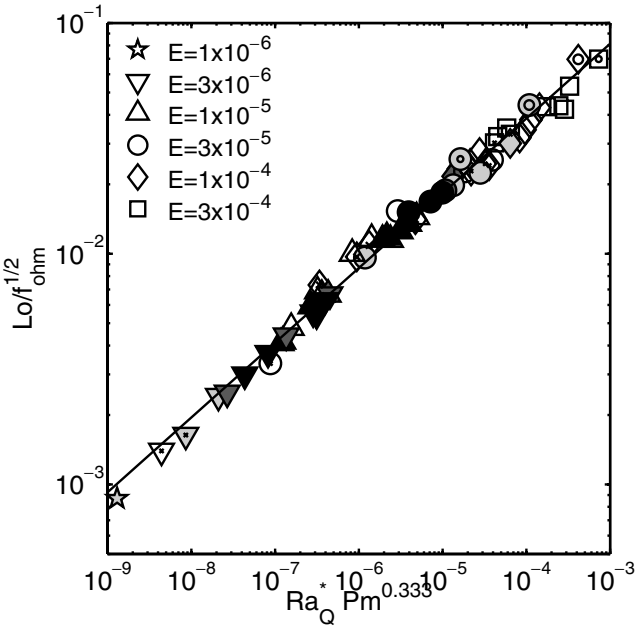

Figure 9. Lorentz number corrected for the relative fraction of Ohmic dissipation versus a combination of modified Rayleigh number and magnetic Prandtl number. Symbols as in Fig. 3.

also depend weakly on the magnetic Prandtl number. Because of the large range of extrapolation required for a planetary application, it is important to verify that the power-law exponents are not biased by dynamo cases that lie far away from an asymptotic regime. For example, an exponent of 0.4 for the relation between Rossby number and modified Rayleigh number has been found for non-magnetic rotating convection, where the main force balance is between inertia, Coriolis force and buoyancy force (Aubert *et al.* 2001). Inertia is assumed to play a small role in planetary dynamos, however, it may still be important in some of our dynamo cases. This might bias the power-law exponent towards a value appropriate for the inertial regime. We test this by fitting only subsets of our dynamo data to a power law.

Table 3. Best-fitting parameters.

	A	α	β	γ	δ
Nu^*	0.0861	0.527	−0.010	0.018	−0.007
Ro	1.159	0.419	−0.131	0.020	−0.028
$Lo/\sqrt{f_{\rm ohm}}$	0.837	0.312	−0.105	0.023	−0.026

Cases with a large value of the scale-sensitive Rossby number Ro_ℓ are more affected by inertial forces than those at low Ro_ℓ. We set a threshold for the modified Rossby number of 0.05, that is, a factor 2.5 below the critical value at which the dipolar dynamo regime breaks down. When we reject all cases above this threshold, retaining 36 models, the exponent to Ra_Q^* for the Rossby number is 0.39 and that for the corrected Lorentz number is 0.36. This is not very different from the exponents obtained when all data are included. When we reject all dynamos with an Ekman number of 10^{-4} or larger, which are presumably more affected by viscous forces than those at lower values of the Ekman number, the power-law exponents relating Ro and $Lo/f_{\rm ohm}^{1/2}$ to the modified Rayleigh number remain unchanged within one percent.

In order to verify that the parameters not included in the fit, the Ekman number and the hydrodynamic Prandtl number, do not affect the dynamo properties significantly we calculate a general least-squares fit of the form

$$Y = A Ra_Q^{*\alpha} Pm^\beta E^\gamma Pr^\delta, \tag{35}$$

where Y stands for any of Nu^*, Ro, or $Lo/f_{\rm ohm}^{1/2}$. The best-fitting exponents are listed in Table 3. Those describing a dependence on the Ekman number or on the Prandtl number differ only very marginally from zero.

These tests suggest that power laws relating the Rossby number and the Lorentz number to the flux-based modified Rayleigh number, with exponents of the order 2/5 and 1/3, respectively, are robust within our range of model parameters and can probably be extrapolated beyond this range.

4 FORCE BALANCE

The scaling laws presented in the previous sections are mainly empirical, that is, they are derived by fitting numerical data. Usually such laws can be understood in terms of a balance of dominant forces or physical effects. We have presented a rationale for the scaling of the magnetic field strength based on the available power that lead to eq. (32). However, to arrive at our final expression (33) we had to resort to the empirical relation between Rossby number and Rayleigh number, for which an explanation is missing so far.

In the so-called mixing length theory for non-magnetic rotating convection a triple balance between buoyancy, Coriolis force and inertia is supposed. A critical point is the value of the characteristic length scale δ. With the simple assumption $\delta \sim D$ the flow velocity is predicted to depend on the 1/3 power of the heat flux (Starchenko & Jones 2002; Stevenson 2003). Aubert *et al.* (2001) invoked different length scales parallel to the rotation axis, $\delta_z \sim D$, and perpendicular to it, $\delta_\phi \ll D$, and obtained with the triple force balance a 2/5 power law for the dependence of the Rossby number on the modified flux-based Rayleigh number. In the dynamo case the presence of the Lorentz force adds complexity to any such analysis. In the magnetostrophic assumption, usually made for dynamos

in an earth-like regime, inertia is replaced by the Lorentz force in the triple balance. Starchenko & Jones (2002) derived a dependence of the magnetic field strength $\sim (Q_B\ \Omega)^{1/4}$ and found an order-of-magnitude agreement with the estimated field inside the Earth and Jupiter. In their analysis they supposed that the characteristic length scale of the magnetic field is independent of the magnetic Reynolds number and fixed the value to $\delta_B \approx r_o/50$ from numerical simulations at $Rm = 200$. However, the inverse dependence of the magnetic dissipation time on the magnetic Reynolds number found by Christensen & Tilgner (2004) in the range of 50–1000 for Rm implies that $\delta_B \sim Rm^{-1/2}$.

Analysing the zonal part of the flow in numerical models, Aubert (2005) found that the zonal velocity scales differently for dynamos and for non-magnetic convection, which can be explained by Lorentz forces playing a significant role in the former case and inertia in the latter. The importance of the Lorentz force seems less clear in our case, where the total velocity and magnetic field are considered. The large variability of the Elsasser number casts some doubt on a basically magnetostrophic balance. However, the conventional Elsasser number (eq. 1) does not take into account that the Lorentz force depends on the length scale of the magnetic field, whereas the Coriolis force does not depend on any length scale, hence Λ may not be a good measure for the relative importance of these two forces. By a simple scaling argument we get the length scale δ_B from Ohmic dissipation: $D_\lambda \sim E_\lambda\, Lo^2/\delta_B^2 \sim f_{\rm ohm}\, P \sim f_{\rm ohm}\, Ra_Q^*$. Using eq. (33), we obtain $\delta_B \sim E_\lambda^{1/2} Ra_Q^{*-1/6}$. The ratio of the Lorentz force term to the Coriolis term in eq. (2) scales as $Lo^2/(\delta_B\, Ro) \sim f_{\rm ohm} E_\lambda^{-1/2} Ra_Q^{*0.42}$. Therefore, our scaling laws suggest a rather variable influence of the Lorentz forces depending on the control parameters. Obviously the Lorentz force must have a significant effect on the flow in every dynamo, because this is the only way how the magnetic field strength can saturate. However, it does not necessarily mean that a global balance with the Coriolis force holds, which is implied in our formula. The spatial distribution of the Lorentz force can be very intermittent (see for example Figure 14 in Rotvig & Jones (2002)), and the balance may be local rather than global. Furthermore, major parts of the Coriolis force and/or the Lorentz force can be balanced by pressure gradients, and only the unbalanced residuals are meaningful in a MAC balance.

4.1 Enstrophy budget

We calculate for several of our models sources and sinks of enstrophy $\boldsymbol{\omega}^2$, which is the 'energy of vorticity' $\boldsymbol{\omega} = \nabla \times \mathbf{u}$. In fluid systems where the Coriolis force plays a significant role, the geostrophic equilibrium usually holds between the Coriolis force and the pressure gradient. However, the dynamics of the system is not controlled by this equilibrium, but by departures from it, where the contributions of other forces play an decisive role. It is, therefore, useful to remove the geostrophic balance from the Navier–Stokes equation by considering the vorticity equation, obtained by taking the curl of eq. (2):

$$\frac{\partial \boldsymbol{\omega}}{\partial t} + \nabla \times (\boldsymbol{\omega} \times \mathbf{u}) - 2\frac{\partial \mathbf{u}}{\partial z} = \frac{Ra^*}{r_o}\nabla \times (T\mathbf{r}) + \nabla \times [(\nabla \times \mathbf{B}) \times \mathbf{B}] + E\nabla^2 \boldsymbol{\omega} \qquad (36)$$

The pressure gradient disappears in eq. (36) and the Coriolis term is reduced to the contribution of the departure from geostrophy $\partial \mathbf{u}/\partial z$. Taking the dot-product of eq. (36) with $\boldsymbol{\omega}$ we obtain the enstrophy equation:

$$\frac{1}{2}\frac{\partial \boldsymbol{\omega}^2}{\partial t} = \underbrace{-[\nabla \times (\boldsymbol{\omega} \times \mathbf{u})] \cdot \boldsymbol{\omega}}_{N_I} \underbrace{-2\frac{\partial \mathbf{u}}{\partial z} \cdot \boldsymbol{\omega}}_{N_C} + \underbrace{\frac{Ra^*}{r_o}[\nabla \times (T\mathbf{r})] \cdot \boldsymbol{\omega}}_{N_B} + \underbrace{(\nabla \times [(\nabla \times \mathbf{B}) \times \mathbf{B}]) \cdot \boldsymbol{\omega}}_{N_L} + \underbrace{E(\nabla^2 \boldsymbol{\omega}) \cdot \boldsymbol{\omega}}_{N_V} \qquad (37)$$

Each of the quantities $N_{I,C,B,L,V}$ gives insight into how the respective forces affect the dynamics of vorticity in the convective dynamo. To get an estimate of the importance of these quantities, unsigned, time-averaged and normalized shell integrals $I_{I,C,L,V}$ are defined as

$$I_{I,C,B,L,V} = \left\langle \frac{\int_{V'} |N_{I,C,B,L,V}|\, dV}{\int_{V'} |N_B|\, dV} \right\rangle. \qquad (38)$$

The angular brackets denote the time-averaging operator, and V' is the spherical shell volume minus the inner and outer viscous boundary layers. These layers are excluded because rigid walls are sources and sinks of enstrophy. $I_{I,C,L,V}$ represents the respective contribution of inertia, Coriolis force, Lorentz force and viscous force in the enstrophy budget, normalized by the driving contribution of buoyancy ($I_B = 1$).

The different contributions to the enstrophy budget are illustrated in Fig. 10 for a reference case. N_B is positive almost everywhere, which correlates with the location of the axial vortices: buoyancy is the main creator of enstrophy. The negative contribution of N_V shows that viscosity is destroying enstrophy mainly near the boundaries and at the edges of axial vortices. The Lorentz force makes a mainly negative contribution N_L. The Coriolis force withdraws enstrophy from the interior of the fluid and creates enstrophy close to the boundaries. This redistribution of enstrophy can be seen as an effect of the Proudman–Taylor constraint. In the interior the fluid the enstrophy associated with gradients of the velocity along $\hat{\mathbf{z}}$ tends to be eliminated and recreated close to the boundary. N_I is sizeable near the inner boundary.

To explore the dependence of the various contributions to the enstrophy budget on the control parameters we have calculated $I_{I,C,L,V}$ for several other dynamo models. The results are shown in Fig. 11, where each of the control parameters is varied separately. The contribution of the Coriolis force I_C is found to be consistently in balance with the contribution of buoyancy $I_B = 1$. Since the integrals are normalized with I_B, they can also be seen as normalized by I_C, and as a logical result, the variations of $I_{I,L,V}$ basically reflect the respective variations of the Rossby, Elsasser and Ekman numbers. The contribution I_L of the Lorentz force is quite variable, suggesting again that the saturation of the magnetic field does not originate in a force balance, but rather in an energy balance. In the case of a non-dipolar dynamo included in Fig. 11(a), inertia is dominating the enstrophy balance, in agreement with our previous assumption that the dipolar dynamo regime breaks down when inertia becomes important.

While the inertial and viscous contributions to the enstrophy budget are usually smaller than those of the Coriolis and buoyancy force, there is not an order-of-magnitude difference. However, we note that by considering a vorticity equation rather than the original Navier–Stokes equation smaller scales are more strongly emphasized. Both the inertial term and the viscous term in the Navier–Stokes equation involve a length scale, whereas the Coriolis term does not. Hence we expect that inertia and viscosity contribute less to a force balance of the flow at large scales.

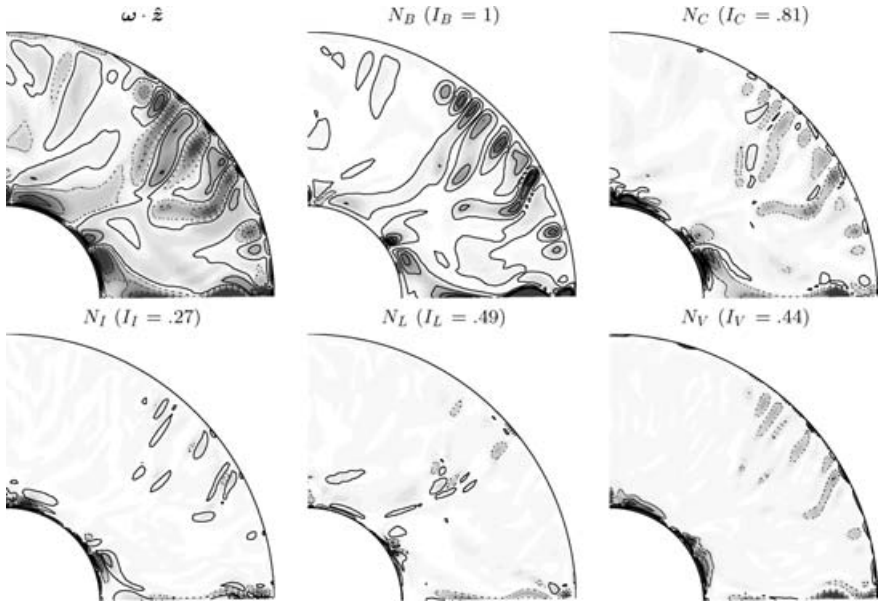

Figure 10. Equatorial cuts of the axial vorticity $\omega \cdot \hat{z}$ (dotted contours: negative values, plain contours: positive values, contour increment: 0.15), and the various contributions to the enstrophy budget (same convention, contour increment: 0.018). $E = 10^{-4}$, $Pm = Pr = 1$, $Ra^* = 0.075$.

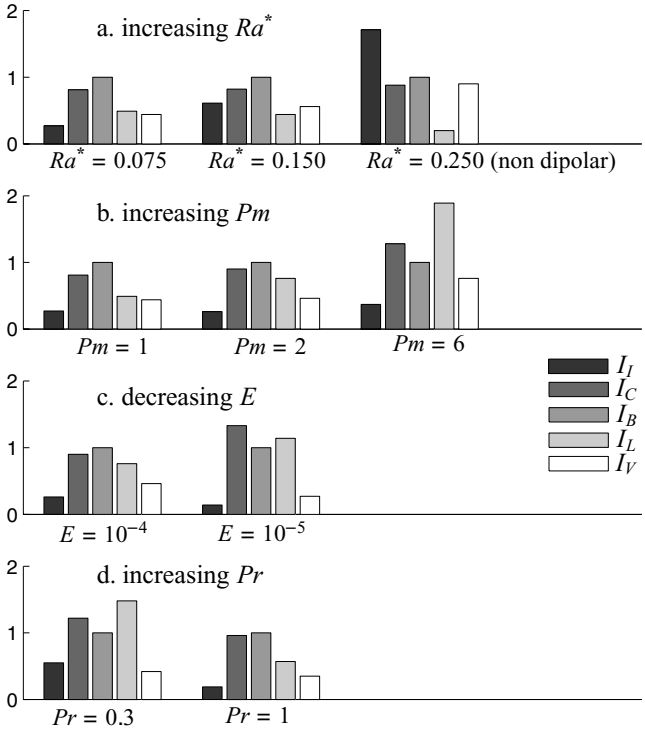

Figure 11. Contributions to the enstrophy budget for various cases. (a) Ra^* is variable ($Pm = 1$, $Pr = 1$, $E = 10^{-4}$). (b) Pm is variable ($Ra^* = 0.075$, $Pr = 1$, $E = 10^{-4}$). (c) E is variable (Ra^* is 10 times supercritical, $Pr = 1$, $Pm = 2$). (d) Pr is variable ($E = 3 \times 10^{-5}$, Ra^* is 10 times supercritical, $Pm = 1$).

4.2 Scaling of the Rossby number

We now attempt to explore the theoretical background for the scaling of the typical value Ro of the velocity. We assume that the thermal fluctuations of typical amplitude δT have an azimuthal size of order δ_φ, different from the characteristic length scale of the flow δ_z in the direction of the rotation axis. In the previous section we have seen that a balance between the curled Coriolis force and the curled buoyancy force generally holds in the enstrophy budget (eq. 37):

$$2\frac{\partial \mathbf{u}}{\partial z} \sim \frac{Ra^*}{r_o}\nabla \times (\delta T \mathbf{r}). \tag{39}$$

An order-of-magnitude analysis yields

$$\frac{Ro}{\delta_z} \sim Ra^* \frac{\delta T}{\delta_\varphi}. \tag{40}$$

Temperature fluctuations and velocity can also be related through an estimate of the convective Nusselt number:

$$Ro\ \delta T \sim Nu^*, \tag{41}$$

hence

$$Ro \sim (Ra_Q^*)^{1/2}\sqrt{\frac{\delta_z}{\delta_\varphi}}. \tag{42}$$

The variation of $\sqrt{\delta_z/\delta_\varphi}$ with the Rayleigh number must account for the difference between the observed scaling exponent of 0.41 and the reference value of 1/2 in eq. (42). Either δ_φ must increase with Ra_Q^*, or δ_z decrease, or both may vary. For non-magnetic convection, Aubert *et al.* (2001) proposed that δ_z/D remains of order one due to the geostrophy of the convective flow, and that δ_φ is determined by a balance between inertia and Coriolis force and increases with the vigour of convection. This theory yields $Ro \sim (Ra_Q^*)^{0.4}$, in close agreement with our empirical results. Because of the strongly variable and often rather small contribution of inertia to the enstrophy budget (Fig. 11), it seems unlikely that the balance between inertia and the Coriolis force can generally be invoked in our dynamo models. Furthermore, we calculated the mean harmonic order $\bar{m}$ in the kinetic energy spectrum, which should be inversely proportional to δ_φ. In models of non-magnetic convection (not reported here), we found indeed a systematic decrease of $\bar{m}$ with the Rayleigh number, consistent with the increase of δ_φ observed experimentally by Aubert *et al.* (2001). In the dynamo cases however, the variation of $\bar{m}$ with the Rayleigh number is smaller and incoherent. This suggests

that the force balance differs between non-magnetic and magnetic cases. We must, therefore, assume that in the dynamos δ_z is reduced when the flow becomes more vigorous, which might be affected by Lorentz forces. However, we did not record the characteristic length scale in z-direction in our models and a more definitive analysis remains a task for the future.

5 APPLICATION TO THE EARTH AND PLANETS

In this section we discuss the scaling laws for the heat flow, flow velocity and magnetic field in physical units and make applications to the geodynamo and other planetary dynamos, assuming that the scaling laws remain valid under planetary conditions.

5.1 Core heat flow

The exponent in the scaling law for the modified Nusselt number (eq. 29) is close to 0.5, and in order to simplify the following discussion, we assume it to be exactly 0.5. With the exponent fixed in this way, the constant in eq. (29) should be adjusted:

$$Nu^* \approx 0.05 Ra_Q^{*1/2}. \tag{43}$$

Casting the scaling law into dimensional form we then obtain

$$Q_{\rm adv} \approx 0.01 \frac{\pi r_o r_i \alpha g_o \rho c \Delta T^2}{\Omega}. \tag{44}$$

A remarkable point about eq. (44) is that the (advected) heat flow is independent of thermal conductivity. Of course, this is a consequence of the existence of a relation between non-dimensional parameters Nu^* and Ra_Q^* that are both independent of thermal conductivity. However, it is surprising that conductivity plays no role because the heat must be conducted through boundary layers at the inner and outer shell boundaries. Obviously eq. (44) cannot hold in the limit of vanishingly small conductivity where the thermal boundary layer thickness must go to zero. The validity of eq. (44) probably requires that the thermal boundary layer extends beyond the Ekman layer. With an Ekman layer thickness of $DE^{1/2}$ and a thermal boundary layer thickness of D/Nu, using eqs (18) and (43) and neglecting the difference between Nu and $Nu - 1$, we arrive at the condition

$$Ra_Q^* < 400 E Pr^{-2}. \tag{45}$$

This condition is satisfied in all numerical models. With the estimates for Ra_Q^* given below it also satisfied in the Earth's core.

Let us assume that convection in the Earth's core is mainly thermally driven. Estimates for the core heat flow vary widely (e.g. Buffett 2002). Taking a value of 2 TW for the advected heat flow and appropriate values for the other parameters ($\alpha = 10^{-5}$, $g_o = 10$, $\rho = 10^4$, $c = 700$, $r_o = 3.48 \times 10^6$, $r_i = 1.22 \times 10^6$, $\Omega = 7.3 \times 10^{-5}$, in SI-units), we can use eq. (44) to estimate a driving (superadiabatic) temperature contrast of $\Delta T \approx 1$ mK. The corresponding density anomaly providing the buoyancy is 10^{-4} kg m^{-3}. The same value has been estimated by Aurnou *et al.* (2003) from a study of vortex-flow driven by a thermal wind inside the core's tangent cylinders.

5.2 Buoyancy flux and inner core growth

Since the buoyancy flux in the Earth's core is poorly constrained, the value of the Rayleigh number Ra_Q^* cannot be calculated directly. However, decent estimates for the characteristic flow velocity in the core have been derived from geomagnetic secular variation. Therefore, we use the relation between Rossby number and Rayleigh number to estimate a value for the latter. A typical velocity of flow near the core's surface obtained by inverting secular variation data is 0.4–0.5 mm s^{-1} (Voorhies 1986; Bloxham *et al.* 1989). Only the large-scale part of the flow is retrieved in these inversions and it is an open question how much energy is present at smaller scales and contributes to the rms velocity. In our models we find that the velocity of the large-scale flow below the Ekman layer near the outer surface, for harmonic degrees ℓ up to 12, is typically of the order of 1/4 to 1/2 of the total rms velocity in the entire shell. Taking this ratio as a rough guide, a better estimate for the true rms velocity in the core may be 1 mm s^{-1}, which gives a Rossby number of 6×10^{-6}. From eq. (30) the flux-based modified Rayleigh number in the core is then obtained as $Ra_Q^* = 3 \times 10^{-13}$.

A somewhat independent estimate of Ra_Q^* is obtained from the scaling relation for the Rossby number related to the zonal part of the flow that has been obtained by Aubert (2005): $Ro_{\rm zonal} \approx 0.9\, Ra_Q^{*1/2}$. The zonal flow contributes significantly inside the Earth's inner core tangential cylinder, but is substantially weaker outside. A characteristic value is 0.1 mm s^{-1} (Olson & Aurnou 1999; Hulot *et al.* 2002). The zonal flow Rossby number of 6×10^{-7} leads to an estimate for the Rayleigh number of $Ra_Q^* = 4 \times 10^{-13}$, very similar to the value derived using the global velocity.

Assuming a core viscosity of $\nu = 2 \times 10^{-6}$ m^2 s^1 and thermal diffusivity of 8×10^{-6} m^2 s^{-1}, which gives $E = 5 \times 10^{-15}$ and $Pr = 0.25$, other parameters of interest have the following values: $Nu^* \approx 10^{-8}$, $Nu \approx 10^6$, $Ra^* \approx 10^{-5}$ and $Ra \approx 10^{23}$. The critical Rayleigh number for non-magnetic convection at this Prandtl number is $Ra_{\rm crit} \sim 2\, E^{-4/3} \approx 2 \times 10^{19}$ (Jones *et al.* 2000), hence convection in the core would be 5000 times supercritical even in the absence of a magnetic field. Our estimate for the degree of supercriticality is fairly similar to that obtained by Gubbins (2001) along different lines of reasoning for 'turbulent' parameters, where his ratio between turbulent and molecular thermal diffusivity is equivalent to our Nusselt number.

If core convection were completely thermally driven, these values of the the Rayleigh number would correspond to a superadiabatic heat flow of 2–3 TW. However, it is believed that most of the driving buoyancy arises from the rejection of the light alloying element from the growing inner core (Loper 1978; Buffett *et al.* 1996). Kutzner & Christensen (2002) found that the properties of chemically driven dynamos, in which the buoyancy flux originates at the inner shell boundary and is zero on the outer boundary, are fairly similar to those of dynamos driven by a fixed temperature contrast. We assume that the same scaling laws hold, with Ra_Q^* replaced by the Rayleigh number based on the buoyancy flux Ra_B^* (eq. 20). Our estimated value for the flux-based modified Rayleigh number of 3–4 $\times 10^{-13}$ translates into a buoyancy flux of $3 - 4 \times 10^4$ kg s^{-1}. The rate of growth of the inner core radius r_i is obtained as

$$\frac{dr_i}{dt} = \frac{Q_B}{4\pi r_i^2 \Delta\rho_{ic}}. \tag{46}$$

$\Delta\rho_{ic}$ is the compositional contribution to the density contrast at the inner core boundary, which is estimated to be in the range 350–700 kg m^{-3} (Gubbins *et al.* 2004). The predicted rate of inner core growth is approximately 0.1 mm yr^{-1}. Assuming for simplicity a constant buoyancy flux, which concurs with a magnetic field strength that did not change substantially over geological time, the age of the inner core $t_{ic} = 4\pi r_i^3 \Delta\rho_{ic}/(3Q_B)$ is obtained as 3.5 ± 1.5 Gyr. The calculated rate of inner core growth is smaller and the suggested inner

core age substantially larger than other recent estimates (Labrosse *et al.* 2001; Nimmo *et al.* 2004), which assumed that a higher heat flux from the core (or higher buoyancy flux) was necessary to drive to geodynamo. With typical values for the relevant thermodynamic parameters, a slightly subadiabatic value of the CMB heat flux is sufficient to let the inner core grow at 0.1 mm yr^{-1} and generate a buoyancy flux at the inner core boundary of the order required by our analysis. The buoyancy flux at the CMB is weakly negative in such a scenario, which should be taken into account for a more quantitative analysis.

We close this section by giving for later purposes the relation between the dimensional characteristic velocity U and the flux, where we set for simplicity the exponent in eq. (30) equal to 0.4 and adjust the constant:

$$U \approx 0.7 \left(\frac{D}{\Omega}\right)^{1/5} \left(\frac{\alpha g_o Q_{\rm adv}}{4\pi r_o r_i \rho c}\right)^{2/5}. \qquad (47)$$

5.3 Core magnetic field

Next we derive a law for the dimensional magnetic field strength by using the dependence of the Lorentz number on the Rayleigh number with a power-law exponent of $1/3$ and no influence of the magnetic Prandtl number (eq. 33). The fraction of Ohmic dissipation in most of our models is in the range of 0.3–0.8. For the Earth's core $f_{\rm ohm} \approx 1$ is usually assumed, based on a ratio of magnetic energy to kinetic energy much larger than one and the high magnetic diffusivity. However, if the kinetic energy is allowed to cascade to much smaller length scales than the magnetic energy, viscous dissipation may still be significant. From our model results we did not find a simple rule of how $f_{\rm ohm}$ varies with the control parameters, but for simplicity we will make the usual assumption that viscous dissipation becomes negligible under core conditions. Replacing again the heat flux by the buoyancy flux, we then obtain for the characteristic value of magnetic induction inside the dynamo region

$$B \approx 0.9\, \mu^{1/2} \rho^{1/6} \left(\frac{g_o Q_B D}{4\pi r_o r_i}\right)^{1/3}. \qquad (48)$$

This scaling law is remarkable, because it predicts that the magnetic field strength is not only independent of the electrical conductivity (or magnetic diffusivity) but also of the rotation rate. It does not imply that these two properties are irrelevant; obviously the diffusivity must be low enough for the magnetic Reynolds number to be supercritical and, as was shown above, the rotational effects must be strong in comparison to the inertial force in order to get a dipole-dominated dynamo at all. However, eq. (48) implies that once these two conditions are satisfied, the precise values of the conductivity and of the rotation rate become unimportant and the magnetic field strength is basically determined by the buoyancy flux and the size of the dynamo.

For the estimated buoyancy flux of $3-4 \times 10^4$ kg s^{-1} an average magnetic field strength in the core of about 1.2 mT is obtained from eq. (48). The corresponding Lorentz number is 6×10^{-5}. Our prediction is somewhat lower than usually quoted values for the core field in the range of 2–4 mT, but the magnetic field strength inside the core is poorly known. It can be estimated via an assumption on how the mean field in the interior relates to the large-scale magnetic field on the core–mantle boundary (CMB). The observed mean dipole field on the CMB is 0.26 mT and the mean field strength in harmonic degrees 1–12 is 0.39 mT (Bloxham & Jackson 1992). In our dynamo models, the magnetic field inside the fluid shell is 3–10 times stronger than the dipole field on the outer boundary (factor $b_{\rm dip}$ in table 2). If such factor applies also to the geodynamo, the core field should be in the range 0.8–2.6 mT. Many of our dynamo models overestimate the contribution of the dipole to the external field, that is, have factors $f_{\rm dip} > 0.8$ as compared to $f_{\rm dip} \approx 0.68$ for the geomagnetic field. $b_{\rm dip}$ is anticorrelated with $f_{\rm dip}$ and for models with earth-like values of $f_{\rm dip}$ the factor $b_{\rm dip}$ is typically 6–7, suggesting a core field strength of 1.7 mT. In a different approach, Zatman & Bloxham (1997) analysed secular geomagnetic variations in terms of torsional oscillations in the core and obtained an rms strength of the magnetic field component B_s pointing away from the rotation axis of ≈0.4 mT. While in some conceptual dynamo models the B_s component is comparatively small (Braginsky 1975), we find that in our models B_s is not significantly weaker than the other components. In this case the inferred $B_s \approx 0.4$ mT corresponds to an overall field strength of about 1 mT. We conclude that our prediction from the scaling laws is in reasonable agreement with independent estimates for the core field strength.

When we use the scaling laws involving a dependence on the magnetic Prandtl number, first eq. (34) to estimate the Rayleigh number in the Earth's core, and in the next step eq. (31) to obtain the magnetic field strength, the results differ substantially. For a value $Pm \approx 2 \times 10^{-6}$ a Rayleigh number $Ra_Q^* \approx 10^{-14}$ is obtained, with a corresponding buoyancy flux of about 1000 kg s^{-1}, a factor of 30 lower than the above estimate. Such a low value seems unlikely. The predicted Lorentz number is 7×10^{-6}, corresponding to a magnetic field strength of 0.13 mT. This is only one-third of the strength of the poloidal field at the core-mantle boundary and can, therefore, be ruled out as a characteristic value for the magnetic field inside the core.

5.4 Jupiter's dynamo

Jupiter's magnetic field is similar to the Earth's field in terms of the ratio of dipole to higher multipole moments and the dipole tilt relative to the rotation axis, but is about 10 times stronger at the surface than Earth's field (Connerney 1981). The internal heat flow is well known, so that we can compare the prediction for the magnetic field strength from our scaling laws with the observed field strength. One complication is that the dynamos in the metallic hydrogen core of these planets are powered by secular cooling, that is, the sources of buoyancy are volumetrically distributed whereas in our numerical model they are located at the inner boundary. To account for this, we replace the inner radius r_i in eq. (48), which refers actually to the radius at which the heat enters, by an effective value of $r_o/2$ and set $D = r_o/2$, thus replacing the term in parenthesis by $g_o Q_B/(4\pi r_o)$. The outer limit of the dynamo region is in the pressure range $P \approx$ 130–160 GPa (Guillot *et al.* 2005), which corresponds to approximately 0.83 of the planetary radius. Probably most of the observed internal heat flow of 5.4 Wm^{-2} (Guillot *et al.* 2005) originates in the deep interior. The factor for conversion of heat flux into buoyancy flux, $\alpha/c_p = \rho/P\,(\partial logT/\partial logP)_S$ is approximately 10^{-9} kg J^{-1} in the dynamo region (Guillot 1999), which leads to a buoyancy flux of 3×10^8 kg s^{-1}. From this and $r_o = 58\,000$ km, $g_o = 30$ m s^{-2} and $\rho = 1400$ kg m^{-3} we obtain a magnetic field strength of 8 mT. The mean dipole field strength of Jupiter, downward continued to r_o, is 1.1 mT. Applying a factor of 6–7 between the field strength inside the dynamo region and that of the dipole on its the outer boundary, as discussed above, leads to an estimate for the internal field in good agreement with the prediction from the scaling law.

A characteristic velocity in Jupiter's dynamo region of approximately 2 cm s^{-1} is predicted from eq. (47), that is, 20 times faster than in the Earth's core. Details of the secular variation of Jupiter's

magnetic field are not known, but Russell *et al.* (2001) determined a change of the dipole tilt by 0.5° between 1975 and 2000. The change of tilt of the Earth's dipole in 25 yr intervals during the time period 1690–2005 according to the ufm1 (Bloxham & Jackson 1992) and IGRF (http://swdcwww.kugi.kyoto-u.ac.jp/igrf) models was highly variable, between zero and 1.3°. The average value of 0.4° change in 25 yr is comparable to the rate of change of Jupiter's dipole. Assuming that the changing tilt represents predominantly magnetic field advection in both cases, the magnitude of the large-scale flow component that advects the dipole field must differ in proportion of the radii of the dynamo regions in Jupiter and Earth, that is, be larger in Jupiter by a factor of about 17, in good agreement with the predicted difference of the rms velocity.

5.5 Magnetic fields of other planets

A similar calculation for Saturn, whose dynamo region is bounded to approximately 60 per cent of the planetary radius, predicts an internal magnetic field strength of about 4 mT, when we assume that roughly one-half of the observed internal heat flow originates in the metallic and deeper layers. In comparison, the observed dipole field projected to the outer boundary of the dynamo region has a mean strength of only 0.15 mT. Either our scaling law fails in the case of Saturn, or the ratio of the internal field strength to the external dipole strength is much larger than in the case of Jupiter and Earth. The very high degree of axisymmetry of Saturn's field (Acuña *et al.* 1981) suggest that the dynamo could be of a different type compared to that in the other two planets. It has been suggested that ongoing fractionation and downward segregation of helium in the outer parts of the metallic region provides energy to drive the dynamo but also leads to a stably stratified conducting region, which may have a strong influence on the magnetic field escaping through this layer (Stevenson 1982a,b). Wicht (personal communication, 2005) found that a dynamo model driven by differential rotation between the inner and outer boundaries of a spherical fluid shell can have a highly axisymmetric external magnetic field. In his models, the ratio $b_{\rm dip}$ is approximately 15.

The magnetic fields of Uranus and Neptune have a strongly tilted dipole that does not dominate compared to higher multipole components, so that our scaling laws do not apply. The relatively low conductivity in the dynamo regions of these planets implies a low Elsasser number Λ. Simple models of dynamos with non-axial dipoles (Aubert & Wicht 2004) suggest that in this case the magnetic field saturates at low values of Λ. Stanley & Bloxham (2004) present a dynamo model where convection is restricted to a relatively thin region overlying a stable fluid layer and which reproduces the observed spectral characteristic of the magnetic field of Uranus and Neptune.

Mercury's field is probably dipolar, but very weak compared to that of the other planets. Could this be due to a low buoyancy flux driving Mercury's dynamo? Because neither the heat flux nor a characteristic velocity in the core are known, we use the magnetic field strength to estimate the buoyancy flux. The size of the inner core is unknown. The scaling laws for thin-shell dynamos or for dynamos with a very small inner core probably differ from those derived here, therefore, we assume a fluid shell of moderate thickness $D = 1000$ km. Arguing along the same lines that we applied to other planets, we estimate from the magnetic field strength of 0.3 μT at the planetary surface a characteristic field strength in the core of 5 μT, which corresponds to a Lorentz number $Lo \approx 4 \times 10^{-5}$. The Rayleigh number obtained from eq. (33) is $Ra_Q^* \approx 10^{-13}$. While this value is similar to our estimate for the Earth, the smaller size and the much slower rotation ($\Omega \approx 1.3 \times 10^{-6}$) make the absolute value of the buoyancy flux inconceivably small, of the order 0.01 kg s^{-1}. The magnetic Reynolds number obtained with eqs (36) and (30) would be around 4, insufficient for sustaining a dynamo. Clearly, weak driving of the dynamo (alone) cannot explain the weakness of Mercury's magnetic field and the explanation may lie in some intrinsic difference between dynamos with a moderate size of the inner core, as in case of the Earth, and dynamos with a very large inner core (Stanley *et al.* 2005) or a very small one (Heimpel *et al.* 2005).

6 DISCUSSION AND CONCLUSIONS

Our analysis shows that dynamos which generate a dipole-dominated magnetic field are preferred when rotational effects on the flow are strong. A strong influence of inertia favours dynamos characterized by weaker magnetic fields dominated by higher multipole components (see also Sreenivasan & Jones 2006). They are less efficient in the sense that they require a higher magnetic Reynolds number. This explains the earlier finding that dipolar dynamos at realistic values of the magnetic Prandtl number $Pm \ll 1$ require also very low values of the Ekman number. Pm can be considered as the ratio of the magnetic Reynolds number to the hydrodynamic Reynolds number. In order to exceed the critical value of Rm, which we find consistently to be approximately 50 for dipolar dynamos, the hydrodynamic Reynolds number has to be very large at low Pm. To 'fight' the associated inertial effects, the rotational constraints must be made very strong, that is, the Ekman number low. If the scaling law for the minimum magnetic Prandtl number at which a dipolar dynamo is possible (eq. 25) remains valid to earth-like values of the Ekman number, the minimum magnetic Prandtl number would be of order 10^{-8}, well below the estimated core values of $Pm \approx 10^{-6}$. Without rotational effects, dynamos are more difficult to obtain at $Pm \ll 1$ (Schekochihin *et al.* 2004; Ponty *et al.* 2005).

In all available numerical geodynamo models several control parameters are far from earth values, mainly because it is not possible to run simulations at the appropriate low values of the viscosity and thermal diffusivity. Whether or not the difference is important depends on the role that diffusive processes play in these models. In the present study we have varied each of the key parameters (E, Pm, Pr, Ra^*) over at least two orders of magnitude and found that within our parameter range the characteristic dynamo properties are at most weakly dependent on the diffusivities. Defining the non-dimensional properties (Rossby number, Lorentz number, modified Nusselt number) and the key control parameter (modified Rayleigh number) in a way that makes them independent of any diffusivity has been very helpful to demonstrate this point. It allows to collapse the data from a substantial range of the 4-D parameter space into a simple dependence on the modified Rayleigh number, at least as a first approximation.

While a simple power law relating the modified Nusselt number to the modified Rayleigh number gives an excellent fit to our results, in the cases of the characteristic flow velocity (Rossby number) and magnetic field strength (Lorentz number) we cannot rule out an additional dependence on other parameters, in particular the magnetic Prandtl number. Although the suggested dependence is weak, it poses a serious problem. Given the large range of extrapolation over five orders of magnitude from our models to planetary values of Pm, the results obtained from the scaling laws with or without a dependence on Pm differ substantially. It is difficult to verify or reject such a dependence based on the numerical results alone;

furthermore, it may change outside the parameter range covered by the model calculations. In the case of scaling the magnetic dissipation time Christensen & Tilgner (2004) tried to resolve the ambiguity by invoking results from the Karlsruhe dynamo experiment (Müller *et al.* 2004), which do not support an additional dependence on the magnetic Prandtl number. Because the flow is strongly constrained in this experiment it cannot be used to test our scaling for the Rossby number and would be of limited help to test the Lorentz number scaling, which through eq. (32) is related to that of the Rossby number. Future dynamo experiments with unconstrained flow in rotating spherical containers (Lathrop *et al.* 2001; Cardin *et al.* 2002) will be better suited to investigate a possible dependence of the magnetic field strength on the diffusion constants or rotation rate.

The rationale for our scaling of the magnetic field strength is not based on the MAC balance, as most previously suggested heuristic scaling laws are (Stevenson 1979,2003; Starchenko & Jones 2002), but on the energetics of the dynamo. These two approaches are not exclusive. Energy is necessarily conserved, but the MAC balance could be satisfied as well. The large variability of the Elsasser number suggests that this is not generally the case, but the Elsasser number may not be adequate to describe the force balance. Therefore, we have calculated the enstrophy budget of several of our models, which eliminates from consideration those parts of the Coriolis or Lorentz forces that are balanced by pressure gradients. The results suggest that the Coriolis and buoyancy forces are globally in balance, however, the total contribution of the Lorentz force is again quite variable. A drawback of studying enstrophy is that it emphasizes the balance for small scales in the flow more strongly than that on large scales. We conclude that the force balance in our models is rather complex. It cannot be understood in terms of a simple MAC balance, in the sense of a close agreement of the mean values of the forces in questions or of their contribution to the enstrophy budget. Whether a MAC balance holds in planetary cores, or in what sense it holds, must be considered an open question. Inertial and viscous forces can play a role provided the flow contains energy at sufficiently short length scales. These scales may be too small for being relevant to the magnetic induction process, however, by inverse cascading of energy (by Reynolds stresses) they can strongly influence the larger-scale flow.

There are some remarkable differences between previously suggested scaling laws and ours. Our scaling of the velocity (eq. 47) is only weakly dependent on the rotation frequency, $U \sim \Omega^{-1/5}$ compared to $U \sim \Omega^{-1/2}$ in case of a MAC balance (Starchenko & Jones 2002; Stevenson 2003). We note that this result depends crucially on the exact value of the exponent in the power law relating the Rossby number to the modified Rayleigh number (eq. 30). A value of 0.5 instead of our preferred 0.4 leads to the MAC balance result. The scaling law for the magnetic field (eq. 48) is completely independent of the rotation rate and the electrical conductivity σ. Under the magnetostrophic assumption it is usually suggested that B is independent of the buoyancy flux Q_B and varies as $B \sim \Omega^{1/2}\sigma^{-1/2}$, based on a balance of Lorentz and Coriolis force expressed by an Elsasser number of order one (e.g. Stevenson 2003). With the different approach of balancing Lorentz force and buoyancy and assuming a fixed length scale δ_B of the magnetic field, Starchenko & Jones (2002) suggested a dependence $B \sim \Omega^{1/4} Q_B^{1/4}$. We would obtain the same result following the reasoning given in Section 3.4 when we assume an exponent of 1/2 instead of 2/5 in the power law for the Rossby number.

Estimates for the buoyancy flux in the Earth's core, which presumably is mostly the compositional flux related to inner core growth, are important because they put constraints on the age of the Earth's inner core, the necessity for heat-producing elements such as ^{40}K in the core, and the degree to which convection in the Earth's mantle is driven by heating from the core (Labrosse 2002; Buffett 2003). Our estimate of 3×10^4 kg s^{-1} based on the scaling of the characteristic flow velocity is in good agreement with results from scaling laws for the zonal flow component alone (Aurnou *et al.* 2003; Aubert 2005). Furthermore, the estimate for the power consumption of the geodynamo of 0.2–0.5 TW obtained from a scaling law of the Ohmic dissipation time (Christensen & Tilgner 2004) can be translated using eqs (20) and (21) into a buoyancy flux of $1.3-3.3 \times 10^4$ kg s^{-1}, in agreement with the other estimates. The rather low values imply that the inner core grows slowly and started to nucleate early in the Earth's history.

Our predictions for the magnetic field strength in the Earth's and Jupiter's core agree well with estimates based on the observed field and reasonable assumptions on the ratio between internal and external field. This is also true for other suggested scaling laws based on simple force-balance arguments. The magnetic fields of Mercury and to lesser degree of Saturn pose a problem for our scaling laws, but also for the other approaches. Mercury and Saturn probably represent different classes of dynamos, whereas Earth and Jupiter basically fall into the same category. The advantage of our scaling laws is that they are based on a fair number of actual dynamo simulations, even if these have been performed at parameters values different from the planetary ones. A drawback is that we can only give a partial theoretical basis for our scaling laws and cannot exclude slightly more complex dependencies that would lead to quite different results when applied to the Earth. However, the fact that Earth and Jupiter fit well with our simple scaling laws supports the view that the present numerical dynamo models operate indeed in the same regime as these two planetary dynamos do. This enhances our confidence that dynamo models are a useful tool to understand not only the bulk properties of planetary magnetic fields but also details of its spatial and temporal behaviour.

NOTE ADDED IN PROOF

Continuing the simulation at the lowest Ekman number of 10^{-6} for another 14 advection times suggested that it has not reached its final equilibrium. Its data should not be used. Omitting this case does not affect any of the scaling laws.

ACKNOWLEDGMENTS

This project is part of the Priority Program *Geomagnetic Variations* of the Deutsche Forschungsgemeinschaft. We are grateful for support through grant Ch77/11.

REFERENCES

Acuña, M.H., Connerney, J.E.P. & Ness, N.F., 1981. Topology of Saturns main magnetic field, *Nature,* **292,** 721–726.

Aubert, J., 2005. Steady zonal flows in spherical shell fluid dynamos, *J. Fluid Mech.,* **542,** 53–67.

Aubert, J., Brito, D., Nataf, H.-C., Cardin, P. & Masson, J.-P., 2001. A systematic experimental study of rapidly rotating spherical convection in water and liquid gallium, *Phys. Earth planet. Int.,* **128,** 51–74.

Aubert, J. & Wicht, J., 2004. Axial versus equatorial dipolar dynamo models with implications for planetary magnetic fields, *Earth planet. Sci. Lett.,* **221,** 409–419.

Aurnou, J., Andreadis, S., Zhu, L.X. & Olson, P., 2003. Experiments on convection in Earth's core tangent cylinder, *Phys. Earth planet. Int.,* **212,** 119–134.

Bloxham, J., 2000a. The effect of thermal core-mantle interactions on the paleomagnetic secular variation, *Phil. Trans R. Soc. Lond.,* A, **358,** 1171–1179.

Bloxham, J., 2000b. Sensitivity of the geomagnetic axial dipole to thermal core-mantle interactions, *Nature,* **405,** 63–65.

Bloxham, J., 2002. Time-independent and time-dependent behaviour of high-latitude flux bundles at the core-mantle boundary, *Geophys. Res. Lett.,* **29,** 1854, doi: 10.1029/2001GL014543.

Bloxham, J., Gubbins, D., Jackson, A., 1989. Geomagnetic secular variation, *Phil. Trans R. Soc. Lond.,* A, **329,** 415–502.

Bloxham, J. & Jackson, A., 1992. Time-dependent mapping of the magnetic field at the core-mantle boundary, *J. geophys. Res.,* **97,** 19 537–19 563.

Braginsky, S.I., 1975. Nearly axisymmetric model of the hydromagnetic dynamo of the Earth I., *Geomag. Aeron.,* **15,** 122–128.

Buffett, B.A., 2002. Estimates of heat flow in the deep mantle based on the power requirements for the geodynamo, *Geophys. Res. Lett.,* **29,** doi:10.1029/2001GL014649.

Buffett, B.A., 2003. The thermal state of the Earth's core, *Science,* **299,** 1675–1677.

Buffett, B.A., Huppert, H.E., Lister, J.R. & Woods, A.W., 1996. On the thermal evolution of the Earth's core, *J. geophys. Res.,* **101,** 7989–8006.

Busse, F.H., Grote, E. & Tilgner, A., 1998. On convection driven dynamos in rotating spherical shells, *Studia Geoph. et Geod.,* **42,** 1–6.

Cardin, P., Brito, D., Jault, D., Nataf, H.-C. & Masson, J.-P., 2002. Towards a rapidly rotating liquid sodium dynamo experiment, *Magnetohydrodynamics,* **38,** 177–189.

Christensen, U.R., 2002. Zonal flow driven by strongly supercritical convection in rotating spherical shells, *J. Fluid Mech.,* **470,** 115–133.

Christensen, U., Olson, P. & Glatzmaier, G.A., 1998. A dynamo model interpretation of geomagnetic field structures, *Geophys. Res. Lett.,* **25,** 1565–1568.

Christensen, U., Olson, P. & Glatzmaier, G.A., 1999. Numerical modelling of the geodynamo: a systematic parameter study, *Geophys. J. Int.,* **138,** 393–409.

Christensen, U.R. & Olson, P., 2003. Secular variation in numerical geodynamo models with lateral variations of boundary heat flow, *Phys. Earth planet. Int.,* **138,** 39–54.

Christensen, U.R. & Tilgner, A., 2004. Power requirement of the geodynamo from ohmic losses in numerical and laboratory dynamos, *Nature,* **439,** 169–171.

Connerney, J.E.P., 1981. The magnetic field of Jupiter: a generalized inverse approach, *J. geophys. Res.,* **86,** 7679–7693.

Glatzmaier, G.A., 1984. Numerical simulations of stellar convective dynamos. I. the model and method, *J. Comput. Phys.,* **55,** 461–484.

Glatzmaier, G.A. & Roberts, P.H., 1995. A three-dimensional convective dynamo solution with rotating and finitely conducting inner core and mantle. *Phys. Earth planet. Inter.,* **91,** 63–75.

Glatzmaier, G.A. & Roberts, P.H., 1995b. A three-dimensional self-consistent computer simulation of a geomagnetic field reversal, *Nature,* **377,** 203–209.

Glatzmaier, G.A., Coe, R.S., Hongre, L., & Roberts, P.H., 1999. The role of the Earth's mantle in controlling the frequency of geomagnetic reversals, *Nature,* **401,** 885–890.

Grote, E., Busse, F.H., Tilgner, A., 1999. Convection-driven quadrupolar dynamos in rotating spherical shells, *Phys. Rev. E,* **60,** 5025–5028.

Grote, E., Busse, F.H. & Tilgner, A., 2000. Regular and chaotic spherical shell dynamos. *Phys. Earth planet. Int.,* **117,** 259–272.

Gubbins, D., 2001. The Rayleigh number for convection in the Earth's core, *Phys. Earth planet. Int.,* **128,** 3–12.

Gubbins, D., Alfè, D., Masters, G., Price, G.D. & Gillan, M.J., 2004. Gross thermodynamics of 2-component core convection, *Geophys. J. Int.,* **157,** 1407–1414.

Guillot, T., 1999. A comparison of the interiors of Jupiter and Saturn, *Planet Space Sci.,* **47,** 1183–1200.

Guillot, T., Stevenson, D.J., Hubbard, W.B. & Saumon, D., 2005. The interior of Jupiter, in: *Jupiter*, pp. 35–37, eds Bagenal, F., Towling, T.E. & McKinnon, W.B., Cambridge Univ. Press, Cambridge.

Heimpel, M.H., Aurnou, J.M., Al-Shamali, F.M. & Gomez Perez, N., 2004. A numerical study of dynamo action as a function of spherical shell geometry, *Earth planet. Sci. Lett.,* **236,** 542–557.

Hulot, G., Eymin, C., Langlais, B., Mandea, M. & Olsen, N., 2002. Small-scale structure of the geodynamo inferred from Oersted and Magsat satellite data, *Nature,* **416,** 620–623.

Ishihara, N. & Kida, S., 2002. Dynamo mechanism in a rotating spherical shell: competition between magnetic field and convection vortices, *J. Fluid Dyn.,* **465,** 1–32.

Jones, C.A., Soward, A.M. & Mussa, A.I., 2000. The onset of thermal convection in a rapidly rotating sphere, *J. Fluid Mech.,* **405,** 157–179.

Kageyama, A., Sato, T. & the Complexity Simulation Group, 1995. Computer simulation of a magnetohydrodynamic dynamo. *Phys. Plasma,* **2,** 1421–1431.

Kono, M. & Roberts, P.H., 2002. Recent geodynamo simulations and observations of the geomagnetic field, *Rev. Geophys.,* **40,** 1013, doi:10.1029/2000RG000102.

Kuang, W. & Bloxham, J., 1997. An Earth-like numerical dynamo model. *Nature,* **389,** 371–374.

Kuang, W. & Bloxham, J., 1999. Numerical modeling of magnetohydrodynamic convection in a rapidly rotating spherical shell: weak and strong field dynamo action, *J. Comput. Phys.,* **153,** 51–81.

Kutzner, C. & Christensen, U.R., 2000. Effects of driving mechanisms in geodynamo models, *Geophys. Res. Lett.,* **27,** 29–32.

Kutzner, C. & Christensen, U.R., 2002. From stable dipolar towards reversing numerical dynamos, *Phys. Earth planet. Int.,* **131,** 29–45.

Kutzner, C. & Christensen, U.R., 2004. Simulated geomagnetic reversals and preferred virtual geomagnetic pole paths, *Geophys. J. Int.,* **157,** 1105–1118.

Labrosse, S., 2002. Hotspots, mantle plumes and core heat loss, *Earth planet Sci. Lett.,* **199,** 147–156.

Labrosse, S., Poirier, J.P. & LeMouël, J.L., 2001. The age of the inner core, *Earth planet. Sci. Lett.,* **190,** 111–123.

Lathrop, D.P., Shew, W.L. & Sisan, D.R., 2001. Laboratory experiments on the transition to MHD turbulence, *Plasma Phys. Control. Fusion,* **43,** A151–A160.

Loper, D.E., 1978. Some thermal consequences of the gravitationally powered dynamo, *J. geophys. Res.,* **83,** 5961–5970.

Müller, U., Stieglitz, R. & Horanyi, S., 2004. A two-scale hydromagnetic dynamo experiment, *J. Fluid. Mech.,* **498,** 31–71.

Nimmo, F., Price, G.D., Brodholt, J. & Gubbins, D., 2004. The influence of potassium on core and geodynamo evolution, *Geophys. J. Int.,* **156,** 363–376.

Olson, P. & Aurnou, J., 1999. A polar vortex in the Earth's core, *Nature,* **404,** 170–173.

Olson, P., Christensen, U.R. & Glatzmaier, G.A., 1999. Numerical modeling of the geodynamo: Mechanisms of field generation and equilibration, *J. geophys. Res.,* **104,** 10 383–10 404.

Olson, P. & Christensen, U.R., 2002. The time-averaged magnetic field in numerical dynamos with non-uniform boundary heat flow, *Geophys. J. Int.,* **151,** 809–823.

Ponty, Y., Mininni, P.D., Montgomery, D.C., Pinton, J.F., Politano, H. & Pouquet, A., 2005. Numerical study of dynamo action at low magnetic Prandtl numbers, *Phys. Rev. Lett.,* **94,** 164502.

Rotvig, J. & Jones, C.A., 2002. Rotating convection-driven dynamos at low Ekman number, *Phys. Rev. E,* **66,** 056308.

Russell, C.T., Yu, Z.J., Khurana, K.K. & Kivelson, M.G., 2001. Magnetic field changes in the inner magnetosphere of Jupiter, *Adv. Space Res.,* **28,** 897–902.

Schekochihin, A.A., Cowley, S.C., Maron, J.L. & McWilliams, J.C., 2004. Critical magnetic Prandtl number for small-scale dynamo, *Phys. Rev. Lett.,* **92,** 054502.

Schekochihin, A.A., Haugen, N.E.L., Brandenburg, A., Cowley, S.C., Maron, J.L. & McWilliams, J.C., 2005. The onset of a small-scale

turbulent dynamo at low magnetic Prandtl numbers, *Astrophys. J. Lett.,* **625,** 115–118.
Simitev, R. & Busse, F.H., 2005. Prandtl-number dependence of convection-driven dynamos in rotating spherical fluid shells, *J. Fluid Mech.,* **532,** 365–388.
Starchenko, S.V. & Jones, C.A., 2002. Typical velocities and magnetic field strengths in planetary interiors, *Icarus,* **157,** 426–435.
Stanley, S. & Bloxham, J., 2004. Convective-region geometry as the cause of Uranus' and Neptune's unusual magnetic fields, *Nature,* **428,** 151–153.
Stanley, S., Bloxham, J., Hutchison, W.E. & Zuber, M., 2005. Thin shell dynamo models consistent with Mercury's weak observed magnetic field, *Earth planet. Sci. Lett.,* **234,** 341–353.
Sreenivasan, B. & Jones, C., 2006. The role of inertia in the evolution of spherical dynamos, *Geophys. J. Int.,* **164,** 467–476.
Stevenson, D.J., 1979. Turbulent thermal convection in the presence of rotation and a magnetic field: a heuristic theory, *Geophys. Astrophys. Fluid Dyn.,* **12,** 139–169.
Stevenson, D.J., 1982a. Interiors of the giant planets, *Annu. Rev. Earth Planet. Sci.,* **10,** 257–295.
Stevenson, D.J., 1982b. Reducing the non-axisymmetry of a planetary dynamo and an application to Saturn, *Geophys. Astrophys. Fluid Dyn.,* **21,** 113–127.
Stevenson, D.J., 2003. Planetary magnetic fields, *Earth planet. Sci. Lett.,* **208,** 1–11.
Stieglitz R. & Müller, U., 2001. Experimental demonstration of the homogeneous two-scale dynamo. *Phys. Fluids,* **13,** 561–564.
Takahashi, F., Matsushima, A. & Honkura, Y., 2005. Simulation of a quasi-Taylor state geomagnetic field including polarity reversals on the Earth simulator, *Science,* **309,** 459–461.
Tilgner, A. & Busse, F.H., 1997. Final amplitude convection in rotating spherical fluid shells. *J. Fluid Mech.,* **332,** 359–376.
Tilgner, A., 1999. Spectral methods for the simulation of incompressible flow in spherical shells. *Int. J. Numer. Meth. Fluids,* **30,** 713–724.
Voorhies, C.V., 1986. Steady flows at the top of the Earth's core derived from geomagnetic field models, *J. geophys. Res.,* **91,** 12 444–12 466.
Wicht, J., 2002. Inner-core conductivity in numerical dynamo simulations, *Phys. Earth planet. Int.,* **132,** 281–302.
Zatman, S. & Bloxham, J., 1997. Torsional oscillations and the magnetic field inside the Earth's core, *Nature,* **388,** 760–763.

APPENDIX A: POWER GENERATION

Here we show that the flux-based modified Rayleigh number is a measure for the power P generated by the buoyancy forces. Denoting the time average by angular brackets and using non-dimensional quantities throughout, we write the averaged eq. (21) as

$$P = Ra^* \int_{r_i}^{r_o} \frac{r}{r_o} \left(\int_S \langle u_r T \rangle \, dS \right) dr, \tag{A1}$$

The surface integral in (A1) is equivalent to the non-dimensional advected heat flux $Q_a(r)$ through a spherical surface at radius r. In general Q_a will vary with r. The conservation of the total (advective and diffusive) heat flux Q can be written by taking the surface integral form of (4) and averaging in time:

$$\frac{dQ}{dr} = \frac{d}{dr} \left(Q_a - E_\kappa \int_S \left\langle \frac{\partial T}{\partial r} \right\rangle dS \right) = 0. \tag{A2}$$

Q, Q_a and P refer here to the time-average values. The total heat flow is constant with radius and by definition equal to the heat flow in a conductive state times the Nusselt number. Using square brackets for the mean on a spherical surface, we can write:

$$Q_a = 4\pi r_i r_o Nu E_\kappa + E_\kappa 4\pi r^2 \frac{d \langle [T] \rangle}{dr}, \tag{A3}$$

Combining (A1) and (A3) we obtain:

$$P = 4\pi Ra^* E_\kappa \left(Nu \int_{r_i}^{r_o} r_i r \, dr + \int_{r_i}^{r_o} \frac{r^3}{r_o} \frac{\langle [T] \rangle}{dr} \, dr \right). \tag{A4}$$

The second integral is negative. It is of order one and, therefore, small compared to the first term in parenthesis when $Nu \gg 1$. The precise result at moderate values of the Nusselt number depends on the radial distribution of the temperature gradient, or in other words, on the partitioning of conductive and advective heat transport with radius. To obtain an approximate expression we evaluate the second integral for a purely conductive temperature gradient $dT/dr = -r_i r_o / r^2$, which assumes that the ratio of advective to conductive heat flow does not change with r:

$$P \approx 2\pi Ra^* E_\kappa \, (Nu - 1) r_i \left(r_o^2 - r_i^2 \right). \tag{A5}$$

Writing the result in terms of the ratio $\eta = r_i / r_o$ and the heat-flux-based modified Rayleigh number we obtain:

$$P \approx 2\pi \eta \frac{1+\eta}{(1-\eta)^2} Ra_Q^* \approx 7.01 Ra_Q^*. \tag{A6}$$

We have recorded the power in our selected dynamo models by evaluating and time averaging the integral (21) and plot it in Fig. A1 against the Rayleigh number Ra_Q^*. The points fall almost perfectly on the line given by eq. (A6). Although the radial temperature distribution certainly deviates from the conductive one, this appears to be of little consequence. However, the good agreement holds only for fully developed convection with $Nu > 2$. In cases with smaller values of the Nusselt number we find that the power is below the value given by eq. (A6).

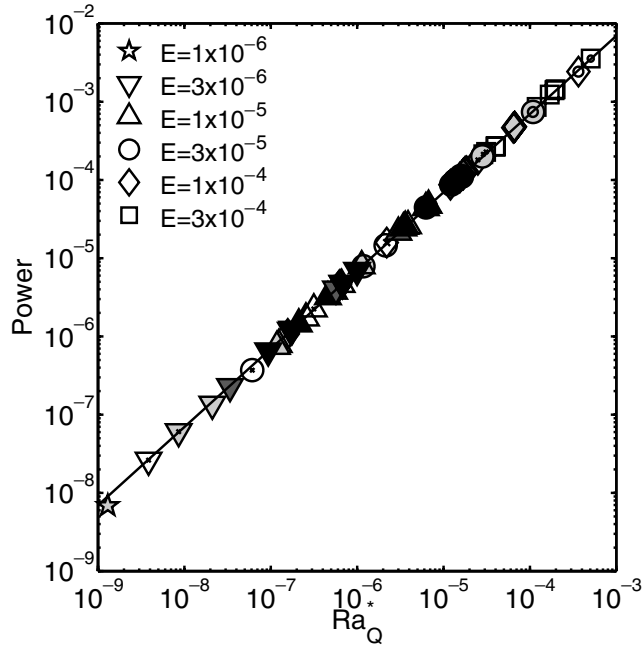

Figure A1. Power versus modified flux-based Rayleigh number. Symbols as in Fig. 3. The slope of the fitting line has been set to one, the constant obtained from a best fit is 6.97.